University of Zurich[UZH]

Zurich Open Repository and Archive
University of Zurich
University Library
Strickhofstrasse 39
CH-8057 Zurich
www.zora.uzh.ch

Year: 2016

Mass fluxes and clay mineral formation in soils developed on slope deposits of the Kowarski Grzbiet (Karkonosze Mountains, Czech Republic/Poland)

Waroszewski, Jaroslaw ; Egli, Markus ; Kabala, Cezary ; Kierczak, Jakub ; Brandová, Dagmar

Abstract: Weathering, mineral formation, and transformation processes along slopes are complex. In cool mountainous regions, undisturbed soil development with a strong vertical leaching element may abruptly change as a result of erosion, accumulation, lateral water fluxes and aeolian input. We investigated soils in the eastern Karkonosze Mountains that have developed on silicatic slope deposits. To date, illite, vermiculite and chlorite are the minerals that have been detected in the clay fraction. Although the climate and parent material should be favourable for the formation of smectites, expandable phases were not verified so far. We investigated if expandable phases could be detected and how they related to elemental fluxes along a short slope sequence (1142–1268 m a.s.l. on the border between the Czech Republic and Poland). Mass balance calculations indicated intensive mineral weathering together with a significant leaching of Mg, Al, Ca and Mn on the shoulder and foot slope positions. In the middle zone, which has a concave or undulating surface shape, however, the mass balances of several elements (Na, K, Al, P) revealed a less pronounced leaching (corresponding to a lower degree of podsolization) and in some cases even accumulation. At all sites, mass balance calculations and detected soil minerals (e.g. the increase in illite towards the surface together with an increase in Al and K) indicate some aeolian input. Kaolinite was detected in all soil horizons. Its concentration slightly increased towards the soil surface. Together with the pronounced leaching of Ca, part of kaolinite originates from plagioclase weathering. Besides being a weathering product of primary minerals, part of the kaolinite is inherited from the parent material and probably is also due to aeolian input. In all soils, illite was being transformed into vermiculite and smectites (through regularly-interstratified illite-smectite phases). In addition, the content of chloritic components which increases with depth indicated their concurrent weathering and transformation into smectites. Amphibole also may have acted as a source of smectites. Not all smectite is being actively formed in the soil. Most likely due to slope processes (cover beds) that affected even the subsoil, some smectite has been transferred along the slope. Part of the smectite also seems to derive from the parent material. Active formation of expandable clay minerals is related to convex and planar landscape forms. This relationship suggests intense element leaching, inheritance from the parent material and cover bed mixing processes have contributed to the presence of smectite. Along the slope, zones with predominant vertical transport (shoulder, foot slopes) may repeatedly be interchanged with zones dominated by lateral transport (undulating slope, concave forms).

DOI: https://doi.org/10.1016/j.geoderma.2015.08.044

Posted at the Zurich Open Repository and Archive, University of Zurich
ZORA URL: https://doi.org/10.5167/uzh-120438
Journal Article
Accepted Version

The following work is licensed under a Creative Commons: Attribution-NonCommercial-NoDerivatives 4.0 International (CC BY-NC-ND 4.0) License.

Originally published at:
Waroszewski, Jaroslaw; Egli, Markus; Kabala, Cezary; Kierczak, Jakub; Brandová, Dagmar (2016). Mass fluxes and clay mineral formation in soils developed on slope deposits of the Kowarski Grzbiet (Karkonosze Mountains, Czech Republic/Poland). Geoderma, 264:363-378.
DOI: https://doi.org/10.1016/j.geoderma.2015.08.044

*Manuscript
Click here to download Manuscript: 5_Manuscript.doc Click here to view linked References

Mass fluxes and clay mineral formation in soils developed on slope deposits of the Kowarski Grzbiet (Karkonosze Mountains, Czech Republic/Poland)

Jaroslaw Waroszewski[a,1], Markus Egli[c], Cezary Kabala[a], Jakub Kierczak[b], Dagmar Brandova[c]

[a]Institute of Soil Science and Environmental Protection, Wroclaw University of Environmental and Life Sciences, 50-357 Wroclaw, Poland

[b] Institute of Geological Sciences, Department of Experimental Petrology, University of Wroclaw, 50-205 Wroclaw, Poland

[c]Department of Geography, University of Zürich, 8057 Zürich, Switzerland

Abstract

Weathering, mineral formation, and transformation processes along slopes are complex. In cool mountainous regions, undisturbed soil development with a strong vertical leaching element may abruptly change as a result of erosion, accumulation, lateral water fluxes and aeolian input. We investigated soils in the eastern Karkonosze Mountains that have developed on silicatic slope deposits. To date, illite, vermiculite and chlorite are the minerals that have been detected in the clay fraction. Although the climate and parent material should be favourable for the formation of smectites, expandable phases have not so far been verified. We investigated if expandable phases could be detected and how they related to elemental fluxes along a short slope sequence (1142 – 1268 m a.s.l. on the border between the Czech Republic and Poland). Mass balance calculations indicated intensive mineral weathering together with a significant leaching of Mg, Al, Ca and Mn on the shoulder and foot slope positions. In the middle zone, which has a concave or undulating surface shape, however, the mass balances of several elements (Na, K, Al, P) revealed a less pronounced leaching (corresponding to a lower degree of podsolization) and in some cases even

[1] Corresponding author. E-mail address: jaroslaw.waroszewski@up.wroc.pl (J.Waroszewski)

accumulation. At all sites, mass balance calculations and detected soil minerals (e.g. the increase in illite towards the surface together with an increase in Al and K) indicate some aeolian input. Kaolinite was detected in all soil horizons. Its concentration slightly increased towards the soil surface. Together with the pronounced leaching of Ca, part of kaolinite originates from plagioclase weathering. Besides being a weathering product of primary minerals, part of the kaolinite is inherited from the parent material and is probably also due to aeolian input. In all soils, illite has being transformed into vermiculite and smectites (through regularly-interstratified illite-smectite phases). In addition, the content of chloritic components which increases with depth indicated their concurrent weathering and transformation into smectites. Amphibole may also have acted as a source of smectites. Not all smectite is actively formed in the soil. Most likely due to slope processes (cover beds) that even affected the subsoil, some smectite has been transferred along the slope. Part of the smectite also seems to derive from the parent material. Active formation of expandable clay minerals is related to convex and planar landscape forms. This relationship suggests that intense element leaching, inheritance from the parent material and cover bed mixing processes have contributed to the presence of smectite. Along the slope, zones with predominant vertical transport (shoulder, foot slopes) may be repeatedly interchanged with zones dominated by lateral transport (undulating slopes, concave forms).

1. Introduction

Clay minerals are good indicators of former and current weathering processes in mountain soils (Reynolds, 1972; Righi et al., 1999; April et al., 2004). Egli et al. (2003a) showed that an understanding of mineral formation, transformation, and weathering rates is fundamental in the analysis of the reactivity of fragile mountain ecosystems. Clays are often used for estimating the degree of soil development (Certini et al., 1998; Fichter et al., 1998; Mirabella and Sartori, 1998; Mirabella et al., 2002; Bonifacio et al., 2009; Mavris et al., 2015). Egli et al. (2001) and Mavris et

al. (2010) verified the applicability of clay mineralogy to track the initial stages of soil formation in proglacial areas. Kabala and Zapart (2012) demonstrated the usefulness of clay minerals to investigate the weathering intensity and the development of a *cambic* horizon formation on moraines of an Arctic glacier. Clay minerals and soil minerals can also be used as pedosignatures for linking soil evolution and landscape development (Mourier et al., 2010; Böhlert et al., 2011; Dahms et al., 2012; Jäger at al., 2015).

Studies of Podzols that developed from acid crystalline rocks in mountain environments have evidenced the presence of vermiculite, illite/vermiculate, illite/smectite, hydroxyl-Al-interlayered vermiculite (HIV) and chlorites (Wilson, 1986; Bain et al., 1990; Dahlgren and Ugolini, 1991; Egli et al., 2003; Kitagawa, 2005; Viennet et al., 2015). Several authors have described different mechanisms of clay mineral formation associated with the podzolization process, including chlorite to smectite transformation (Wilson, 1999) or smectite and mixed-layered mineral formation at the expense of biotite (Mavris et al., 2011). In addition, imogolite and poorly crystalline phases such as allophone formation have frequently been described (Wada, 1989; Ugolini and Dahlgren, 1991). Most of these studies were conducted in soils developed on more or less homogeneous parent materials (Righi et el., 1999, Egli et al., 2008); whereas in Central European low-/mid-mountains soils are often either polygenetic (Waroszewski et al., 2013, Geitner et al., 2014) or developed from stratified slope deposits (Migoń and Kacprzak, 2014; Waroszewski et al., 2015a, Waroszewski et al., 2015b). Selective and non-selective slope transport produces a heterogeneous sediment differing in petrography and texture which directly or indirectly affects soil formation, morphology and soil-plant interactions (Kleber and Terhorst, 2013); thus, this may also influence the weathering rates, clay formation and transformation processes.

Illite has traditionally been recognized as a main component of the clay fraction in soils of the Karkonosze Mountains (Szerszeń, 1974; Bogda, 1981; Bogda et al., 1998). Also, biotite to vermiculite transformation has been described (Kowalinski et al., 1967; Kabala, 2005). The

presence of smectite has, however, not been confirmed, although the weathering environment, such as strong elemental leaching (Kitagawa, 2005), would be favourable for its formation and precursor minerals such as mica are present. The clay mineralogy of the mountain soils of Central Europe, particularly on slope covers, is still poorly investigated (Kacprzak and Derkowski, 2007).

With this investigation, we attempt to improve the understanding of soil and clay mineral formation in these environments and to answer the question as to under which conditions smectites might or might not be encountered. As such, we aimed at investigating mass fluxes and the formation/transformation of clay minerals in soils under different leaching conditions within a slope on acidic metamorphic rocks (mica schists). A particular focus was given to the detection of semectites and their relation to soil evolution along a toposequence.

2. Study area and sampling sites

The study was carried out on the Czech-Polish border, in the Karkonosze Mountains, the highest part of the Sudeten Mountains (Fig.1). The main ridge (1400 – 1450 m a.s.l.) of the Karkonosze Mts is a plateau with a WNW-ESE orientation. The northern part of the Karkonosze Mts borders with the Jelenia Góra Basin (350 – 500 m a.s.l.) and the southern part is bounded by deep river valleys (Engel et al., 2010; Migoń, 1999). The Karkonosze Mountains consist of Carboniferous granite in their central part, whereas the outer parts are built of metamorphic Pre-Cambrian/Old-Paleozoic metamorphic rocks (gneiss, mica schists, amphibolite schists, etc.). The current relief of the Karkonosze Mountains is the result of weathering and denudation during the Teritary and the Pleistocene glaciations and related mass movements. The Pleistocene Scandinavian ice-sheets reached the foothills of the Sudeten Mts on two occasions: during the San II (Mindel, Pre-Illinoian; MIS stage 12) and Odra (Riss; Illinoian; MIS stage 6) glaciations. During that time, the permanent snow cover was at lower altitudes which promoted snow accumulation in the glacial cirques; as a consequence, mountain glaciers started to develop. The last glacial maximum (LGM)

and late glacial oscillations (Younger Dryas) of the mountain glaciers in the Karkonosze Mountains correlate with the glaciations of the Alps and the Bavarian/Bohemian Forest (Engel et al., 2014). Severe and long-lasting periglacial conditions during the Pleistocene favoured physical weathering and cryogenic slope processes (Migoń and Traczyk, 2000).

The spatial distribution of soils in the Karkonosze Mountains is a function of altitude (climate) and geology resulting in a clear vertical soil zonality. Haplic/Albic Luvisols are present up to 750 m a.s.l., usually on the fine-textured colluvia. The zone between 500 and 800 m a.s.l. is characterized by Dystric/Alumic Cambisols (usually skeletal) developed from granite or gneiss regolith. In the upper forest zone (800 – 1000 m a.s.l.), Albic/Entic Podzols prevail with a high content of rock fragments. Depending on the surface relief between 1000 and 1200 m a.s.l., Podzols become either (1) extremely skeletal when developed on former rock glaciers and block covers (Hyperskeletic Podzols) or (2) increasingly wet if situated on plateaus (Stagnic/Histic Podzols). Histic Podzols and Histosols dominate the zone between 1200 and 1400 m a.s.l. Above an altitude of 1400 m a.s.l., only Lithic Leptosols, Hyperskeletic Leptosols and Skeletic Ragosols can be found (Kabala et al., 2013).

The sampling sites were located in the Kowarski Grzbiet (Střeha), which belongs to the Kowary metamorphic unit (eastern Karkonosze Mts, Aleksandrowski et al., 2013). This area has never been covered by continental or mountain glaciers. However, a strong influence of periglacial conditions was assumed (Jahn, 1963). The Kowarski Grzbiet (Střeha) is a 4-km-long ridge, asymmetrically lifted with an almost completely aligned plateau. It is made of gneiss and mica schist, with local inclusions of chlorite schist, amphibolite schist and quartzite (Aleksandrowski et al., 2013). Waroszewski et al. (2010) recognized that the slope deposits are the parent material for Podzols in the Kowarski Grzbiet. They described remarkable differences in soil morphology as a function of the (1) sandy, hyperskeletic top layer and (2) loamy-skeletic dense basal layer.

125 Mean annual precipitation for this region varies between 900 mm in the foothills, and up to 1350
126 mm on the upper slopes. Mean annual air temperature ranges between 7°C at 600 m a.s.l. and 1 –
127 2°C at 1600 m a.s.l. The duration of snow cover reaches about 200 days per year on the highest
128 peaks (Sobik et al., 2013). The present study was performed in a narrow section of the mountain
129 range (1142 – 1268 m a.s.l.); thus, the climatic conditions along the investigated slope do not
130 include high variability. The vegetation at the sampling sites is dominated by *Picea abies* in the tree
131 layer and *Vaccinium myrtillus* on the forest floor, accompanied by grass species including *Poa*
132 *nemoralis*, *Agrostis capillaries*, *Agrostis canina*, *Poa trivialis*, and *Festuca pratensis*.
133
134 **3. Materials and methods**
135 3.1. Field procedures
136 Four soil profiles were dug along a toposequence (about 450 m long) on a SE-facing slope
137 of the Skalny Stół (1270 m a.s.l., the highest peak of the Kowarski Grzbiet) at an altitude of 1142 –
138 1268 m a.s.l. The site characteristics are presented in Table 1. The soils (Tab. 2) were described
139 according to FAO Guidelines (2006) and the soil reference groups were established using the WRB
140 classification (IUSS working group WRB, 2014). The slope gradient was measured in the field
141 using a clinometer and than rechecked based on the DEM data. Approximately 2 kg of soil material
142 was taken from each soil horizon. Prior to measurements, the samples were dried, gently crushed
143 and passed through a 2 mm sieve. In addition, undisturbed soil samples were collected using steel
144 cylinders to estimate soil bulk density. In some cases (caused by a high skeleton content that
145 disabled the use of cylinders), soil bulk density was determined by excavating holes (and weighing
146 the excavated material) that were backfilled with a measurable volume of quartz sand. To check the
147 geological composition, at least 40 rock fragments per soil profile were crushed to enable a
148 petrographical classification. Stones with a diameter of at least 15 cm were chosen for thin section
149 preparation.

150

151 3.2. Description of rock thin sections

152 Petrographic description of the polished thin sections of dominant rocks was carried out
153 using a Leica DM2500P optical microscope in transmitted and reflected light. The modal
154 composition of the studied rocks was estimated by point counting using the freeware software
155 JMicroVision v1.2.7.

156

157 3.2. Soil analyses

158 After sample pretreatment with 3% H_2O_2 and dispersion with hexametaphosphate, particle-
159 size distribution was performed using sieves (sand fraction) and the hydrometer method for the silt
160 and clay fraction (Van Reeuwijk, 2002). Soil pH was potentiometrically measured in a 1:2.5
161 (soil:distilled water) suspension. Soil organic carbon (SOC) content was determined with the dry
162 combustion method using CO_2 spectroscopic measurements (Ströhlein CS-mat 5500 analyzer).
163 Exchangeable ions (Ca^{2+}, Mg^{2+}, K^+, Na^+) were extracted with 1 M ammonium acetate at pH = 7.
164 Amorphous, poorly crystalline and crystalline Fe and Al forms were determined with the dithionite
165 and oxalate extractions (McKeague et al., 1971). Cation concentrations in the extracts were
166 measured via atomic absorption spectroscopy (AAS) and inductively coupled plasma (ICP-OES).

167 Elemental composition (Si, Al, Ti, Fe, K, Na, Ca, Mg, Mn, P, Cl, and S) was measured
168 using X-ray fluorescence (XRF). Soil material was milled to 50 μm in a tungsten carbide disc swing
169 mill (Retsch® RS1, Germany). Thereafter, the material was weighed into plastic cups with Prolen®
170 foil at the bottom and analysed with an energy dispersive X-ray fluorescence spectrometer
171 (SPECTRO X-LAB 2000, SPECTRO Analytical Instruments, Germany).

172

173 3.3. Mass fluxes

The long-term weathering rates of soils were derived from the calculations of enrichment/depletion factors determined using immobile element contents (Brimhall and Dietrich, 1987; Egli and Fitze, 2000). In this investigation, Ti was used as an immobile element. Although some studies indicate that Ti might be mobile to some extent in weathering environments (Cornu et al., 1999), other 'stable' elements such as Zr are also criticised due to grain corroding caused by surface dissolution (Balan et al., 2001). Therefore, we followed the statement of Stiles et al. (2003), who concluded that Ti is better suited for mass-balance calculations during pedogenesis, as Ti has higher concentrations and is enriched in the clay fraction. The ratio can be used as a weathering index: the lower the ratio (Ti/Ca), the higher the degree of weathering (Dahms et al., 2012).

Relative elemental losses in the soil column can be calculated using the open-system mass transport function $\tau_{j,w}$ (Chadwick et al., 1990):

$$\tau_{j,w} = \left(\frac{C_{j,w} \cdot C_{i,p}}{C_{i,w} \cdot C_{j,p}} \right) - 1 \quad (1)$$

where: i denotes the immobile element (Ti), $C_{j,p}$ (g/kg) is the concentration of element j in the unweathered parent material, and $C_{j,w}$ is the concentration of element j in the weathered product (g/kg).

3.4. Clay mineralogy

The mineralogy of the clay fraction was determined after removal of organic matter and, in some cases (mostly from Bh and Bhs horizons), iron oxides. Oriented specimens on glass slides were analysed via X-ray diffraction (XRD) using Cu–Kα radiation from 2 to 15°2θ with steps of 0.02°2θ at 2 s/step. The following treatments were performed: Mg-saturation, ethylene glycol solvation (EG), and K-saturation. After an initial XRD scan, the K-saturated samples were heated

198 for 2 h at 335 and 550°C, and rescanned after each heating step. The *d*(060) region was studied on
199 randomly oriented samples that were step-scanned from 58 to 64°2θ with steps of 0.02°2θ at 10
200 second intervals using a Bruker AXS D8 Advance (CuKα). In addition, a scan from 2 to 80°2θ
201 (with steps of 0.02°2θ) was performed.
202 Digitised X-ray data in the range of 2 to 15°2θ were corrected for Lorentz and polarisation factors
203 (Moore and Reynolds, 1997). Diffraction patterns in the range of 2 to 15°2θ and 58 to 64°2θ were
204 fitted by the Origin™ PFM program using the Pearson VII algorithm. Background values were
205 calculated by means of a non-linear function (polynomial 2nd order function; Lanson, 1997).
206 To check the presence of kaolinite and imogolite-type materials, DRIFT (Diffuse Reflection
207 Infrared Fourier Transform; Bruker, Tensor 27) measurements were carried out from 250 to 4000
208 cm^{-1}. About 30 mg of clay material and 270 mg of KBr were homogenised in a mill using a fine
209 ball-mill (Zr) for 30 s and at 10 rpm. Prior to measurement, the samples were dried in an oven at
210 70°C for 2 hours. The individual spectra were normalised using OPUS 6 software. The FT-IR
211 spectra of soil clays in the OH-stretching region (4000 – 3200 cm^{-1}) were, furthermore, normalised
212 (using the mininum-maximum method) and then compared to each other. This enables the detection
213 of relative changes in the abundance of kaolinite.
214
215 **4. Results**
216 4.1. Bedrock identification and rock mineralogy
217 The mica schist had a light grey color and was typically lustrous at the foliation surface. It is
218 present in the coarse skeleton of the soils. The mica schist was characterized by oriented mica
219 crystals and by a lepidogranoblastic texture (Fig. 3). The rock material contained quartz, muscovite
220 and chlorite as its major minerals, whereas the minor and accessory constituents were biotite,
221 garnet, sphene, tourmaline, zircon and opaques. The schists had alternating layers consisting of
222 quartz grains up to a thickness of 0.5 mm and mica flakes up to 1 mm (Fig. 3b). Locally, within the

mica layers, a larger amount of chlorite was observed (Fig. 3c and 3d). The schist has experienced some deformation, as evidenced by the clearly visible cleavage in some parts of the rock. Quartz occurred as a major component. It formed anhedral isometric crystals with a size ranging from 0.1 to 0.5 mm. Muscovite was present as subhedral flakes occurring almost exclusively within the mica layers. The size of individual muscovite crystals reached 1 mm. Chlorite and biotite occur within the mica layers as subhedral flakes with a size of up to 0.3 mm and 0.4 mm, respectively. Garnets are isometric, showing subhedral porphyroblasts within quartz or mica layers and reach a size of up to 1 mm. Garnet crystals were strongly weathered, fractured and overgrown with chlorite and secondary brown opaque minerals (Fig. 3c, 3d). Sphene was present exclusively within mica layers, where it formed subhedrally elongated crystals up to 0.25 mm in length. Tourmaline euhedral crystals had a size of about 0.3 mm and showed a trigonal cross-section outline and zoning (Fig. 3c, 3d). Tourmaline crystals usually had a size of up to 0.3 mm. Opaque minerals occurred as two varieties. Black opaques formed anhedral crystals of approximately 0.1 mm in thickness. Brown opaques represented secondary phases that were formed due to garnet and/or black opaque alteration. Zircon euhedral crystals were smaller than 0.1 mm and visible as dark brown to black pleochroic haloes within biotite flakes.

Other rock fragments that were present in the soil profiles had a quartzite composition. Macroscopically, the quartzite varied in color from grey to white. The quartzite was mostly composed of rounded, anhedral, isometric quartz grains of a size between 0.1 to 0.5 mm. The small quartz grains formed a siliceous matrix (Fig. 3a) for the larger (3 to 8 mm) irregular and anhedral crystals of quartz. These larger grains are characterized by an undulatory extinction, a common feature observed in deformed rocks. Small (< 0.01 mm) gas and/or liquid inclusions were common within quartz grains. These inclusions were arranged in more or less parallel lines. Opaques were the only accessory minerals within the quartzite. They formed subhedral to euhedral crystals with a size of up 0.5 mm.

248

249 4.2. Soil characteristics

250 Generally, the thicknesses of organic layers were in the range of 8 – 20 cm (Table 2). The
251 uppermost mineral horizons were bleached due to podzolization, thus having a grey or greyish-
252 brown colour. Partially reducing conditions, related to water stagnation, were found in the E
253 horizons. In profile KH2, subsurface water flow (in May) was evident at the contact of the E to the
254 Bh horizon. The eluvial horizons contained 10 – 30% rock fragments. The thickness of the eluvial
255 horizons varied between 7 and 18 cm without any particular trend along the slope catena. The
256 underlying dark brown Bh/Bhs horizon usually had a subangular, weak to moderate soil structure
257 and a friable consistency. The skeleton content in Bh horizons increased to 50-70%. The lowermost
258 BC horizons were in general more reddish or yellowish and more compacted and friable to firm,
259 compared to adjacent horizons. Soil structure was blocky angular or platy. Rock fragments
260 accounted for up to 90% of the soil mass, and the orientation of the clasts was mostly horizontal.
261 The bulk density of the topsoil horizons varied between 0.67 and 1.25 g cm^{-3}. With depth, bulk
262 density increased in all profiles up to 1.39 g cm^{-3} (BC horizon).

263 In general, all soils were acidic throughout the profile (Table 3). Organic carbon was found
264 to relatively great depths and indicated partially intense translocation (podzolisation) processes. The
265 topsoil layers, except the AE horizon in profile KH3, were strongly depleted in oxalate-extractable
266 Fe and Al. Amorphous iron (Fe_o) was a main fraction of the whole pedogenic forms, as exemplified
267 by the Fe_o/Fe_d ratio, which oscilated within the range of 0.52 and 0.97 (Table 3). Although the soils
268 are located on the same slope and developed in a similar altitudinal (climate) zone and parent
269 material, some differences in particle size distribution were evident. The soil material seems to be
270 relatively homogenous throughout the profiles of KH1 and KH2, with 47 – 52% in the sand and 44
271 – 50% in the silt fraction. A more variable texture, evidenced by a change in the fine silt and fine
272 sand fractions, was found in profile KH3 (Table 4). Profile KH4 had a relatively uniform particle

size distribution with a sandy loam texture throughout the profile. However, it clearly contains less silt (26-38%) and more fine and very fine sand compared to the profiles in the upper-slope (Table 4).

The investigated Podzols and Cambisols developed on slope materials (cover beds) that showed some variations in their coarse fragments and silt content. The upper layers were characterized by a lower rock clast content (10 – 30%) and a silt content of up to 50%, while the basal layer had a significantly higher share of skeleton (60 – 90%) and lower silt content (Table 4). A special case is the topsoil of profile KH3, where silt reached 68%; such an enrichment could be related to erosion (near-surface) and accumulation processes.

4.3. Geochemistry and mass fluxes

The elemental composition of the soils reflects the presence of mica schists in the bedrock. Consequently, the SiO_2 (45.9 – 77.0%) and Al_2O_3 (11.6 – 18.3%) content is high. The eluvial horizons are enriched in Al, Na and K, and depleted in Mg, Ca, Mn and Fe. In particular, the Fe content is around 1.5% in the E horizons and up to 11% in the Bh/Bhs horizons (Table 5). Its pattern is controlled by podzolization.

Open-system mass transport functions τ are reported as a function of soil depth in Table 6 and in Figures 4 and 5. Two important assumptions concerning elemental components are required in mass balance calculations using immobile elements (White, 1995; Egli et al., 2001). The first involves the determination of the composition of the parent material. For soils developed at sites on bedrock, the potential errors are confined to local heterogeneities in bedrock composition. The estimation of the initial composition becomes more difficult when soils have developed on sedimentary parent materials such as cover beds. For such deposits, the least weathered horizon in the soil profile is assumed to be the parent material. Consequently, the gains and losses are calculated in relation to the lowermost and least weathered soil horizon. Element losses are

298 observed in all upper horizons of profiles KH1 and KH4. The most intense leaching was found in
299 the E horizon for Fe, Mn, Ca and Mg (Fig. 4 and 5). Also in the Bh horizon, the values were often
300 negative (except for Fe in KH1). Negative mass balance values of up to 75% were found for Mn
301 and Ca in the eluvial horizons of profiles KH2 and KH3. However, an enrichment of P, Al, K and
302 Na (Fig. 4; Table 6) was measured in the uppermost horizons.
303 The highest (K+Ca)/Ti ratios were measured in the middle part of the slope (Table 5). In
304 profiles KH2 and KH3 the ratio decreased with depth, whereas in profiles KH1 and KH4 it was
305 higher in the topsoil and the BC horizon and lowest in the Bh horizon.
306
307 4.4. X-ray diffraction of the clay fraction
308 The investigated clay fraction (<2 μm) is dominated by quartz, mica, vermiculite, kaolinite,
309 chlorite and interstratified minerals (Table 7, Fig. 6). Smectite or interstratified mica-smectite
310 minerals were also detectable. The main difference in soil mineralogy between the soil horizons (E,
311 Bs/BC) is reflected in the secondary phyllosilicate composition (Table 7). As an example, the Mg-
312 saturated clay sample from the E horizon of soil profile KH2 exhibited distinct peaks at 1.43, 1.16,
313 1.01 and 0.71 nm (Fig. 7). Furthermore, small peaks near 2.06 and 1.04 were detectable. Following
314 EG-solvation, the peaks (or part of them) at 1.43 and 2.06 nm shifted to lower angles at 2.30 and
315 1.65 nm. Potassium saturation caused the peak at 1.43 and 1.16 nm to contract to 1.12 and 1.01 nm.
316 After heating at 335 °C, a dominant peak at 1.01 nm was measured. A very minor component
317 persisted at 1.4 nm even after heating at 550 °C. In this sample, two low-charge expandable
318 minerals could be indentified. The peak at 1.65 nm (after EG-solvation) can be attributed to the
319 d_{001}* of smectite. The shift of the 2.06 nm peak (Mg-saturation) to 2.30 nm (EG-solvation) is a
320 regularly-interstatified mica-smectite (with a d_{002}* near 1.2 nm). In addition, mica was also present
321 (peak at 1.01 nm). Possibly, a minor proportion of interstratified chlorite-smectite could have
322 contributed to the large shoulder between 1.41 and 1.65 nm (similar to that in the other surface

323 samples). Clear evidence is, however, missing (no change in the 0.71 nm peak after EG solvation;
324 the peak near the 0.498 nm was not investigated; Hubert et al., 2009). The Mg-saturated clay
325 sample from the BC horizon of profile KH2 exhibited an XRD pattern with peaks centered at 1.45,
326 1.27, 1.02 and 0.72 nm. With EG-solvation, a peak at 1.67 nm was detectable. A portion of the 1.45
327 nm peak shifted towards 1.02 and 1.12 nm with heating treatment at 335 °C (Fig. 7). Another part
328 remained near 1.4 nm. Subsequent heating treatment at 550 °C did not noticeably change the XRD
329 pattern. The peak at 1.27 nm (Mg-saturation) could therefore represent an interstratified HIV-mica
330 and/or vermiculite-mica. Chlorite was present in a significant concentration due to the persistence
331 of a peak at 1.4 nm even after the heat treatments. After EG-solvation, smectite was again identified
332 by the peak at 1.67 nm.
333 Pronounced and sharp XRD peaks were denoted at 0.71 or 0.72 and 1.01 nm for the other samples
334 from the E, Bh and BC horizons. The peak at 1.01 nm was attributed to mica (illite), while those at
335 0.71 and 0.72 nm were assigned to kaolinite (the 0.71 nm peak disappeared after heating at 550°C)
336 and chlorite (persistence of the 1.42 nm position after heating at 550°C in some samples; data not
337 shown). In the uppermost soil horizon, chlorite was mostly absent (no or almost no peak around 1.4
338 nm after heating at 550 °C). With increasing soil depth, the peak near 1.4 nm (550 °C) was more
339 pronounced; and subsequently, the proportion of chlorite increased with increasing soil depth (Fig.
340 7). The uppermost horizons all showed some smectite with peaks after EG-solvation near 1.66 to
341 1.70 nm (Fig. 8). Particularly in the E horizon of profile KH1, two swelling phases were present,
342 indicated by a regularly-interstratified mica-smectite (indicated by a peak at 2.67 nm (d_{001}*) and
343 1.34 nm (d_{002}*); Fig. 8) and smectite (1.70 nm). The proportion of mica and smectite in the
344 regularly-interstratified mica-smectite was close to a 1:1 ratio (Moore and Reynolds, 1997).
345 For all subsoil samples, a peak at 1.66 to 1.70 nm could be modelled after EG-solvation (Fig. 9).
346 This indicates that some smectite is also present in the subsoil or parent material. Besides mica,
347 kaolinite and chlorite, and also some regularly-interstratified mica-HIV or mica-vermiculite were

348 detectable (Table 7, Fig. 9). In the lower horizons (Bs, BC), a broad peak near 1.4 nm was detected
349 (Fig. 9). Since a small part of this peak shifted to 1.01 nm after K saturation, a minor amount of
350 vermiculite is present. In some cases traces of amphibole (0.85 nm) were also detectable (Fig. 9).
351 The soils at a convex and planar slope position and at the mountain ridge showed a considerable
352 amount of smectite in the topsoil. At these positions, the element leaching rates were elevated
353 compared to profile KH3.
354 The XRD patterns in the d_{060} are presented in Figure 10. X-ray profile fitting enabled the separation
355 of a quartz peak near 0.1544 nm and trioctahedral species at 0.155 to 0.156 nm and 0.1539 to
356 0.1541 nm that can be attributed to biotite and chlorite, respectively (Moore and Reynolds, 1997). A
357 small peak was discernible at 0.1524 nm due to Fe-rich dioctahedral minerals (Fanning et al., 1989);
358 the other dioctahedral species were represented by the peaks in the 0.1515 – 0.1490 nm region. The
359 peak near 0.1491 nm seems to represent kaolinite. The analysis of the d_{060} region shows that the
360 proportion of dioctahedral was higher in the topsoil compared to the suboil. Subsequently,
361 trioctahedral species decreased when approaching the soil surface.
362
363 4.5. DRIFT measurements
364 The peaks at 375 cm^{-1} 915 cm^{-1}, 3620 cm^{-1} and 3694 cm^{-1} (Farmer, 1974) confirmed the
365 presence of kaolinite in all soil horizons (Fig. 11). Kaolinite seems to slightly increase towards the
366 soil surface (Fig. 11c). Besides minerals, organic functional groups were detected, such as
367 vibrations of methyl (-CH_3) and methylene (=CH_2) aliphatic compounds (2900 – 2930 cm^{-1} in the
368 AE and E horizons). Additional organic components were carboxylic groups (-COOH), aromatic
369 compounds and conjugated ketones (1620 cm^{-1}), and the C-O stretching of polysaccharide observed
370 at 1080 cm^{-1} (Stevenson, 1994; Senesi et al., 2003). Weakly developed Si-O stretching bands
371 around 1030 cm^{-1} were attributed to newly-forming dioctahedral phases (Mavris et al., 2011) and
372 the vibration found at circa 1020 cm^{-1} was typical for trioctaherdral sheet silicates. Quartz was

identified by the doublet peaks at 780 and 800 cm^{-1} (Farmer, 1974). Chlorite was detected around 750 cm^{-1} in profiles KH2 and KH4. The peaks around 474 and 531 cm^{-1} corresponded to illite or muscovite (Farmer, 1974; Fig.11).

5. Discussion

The thickness of the diagnostic horizons and the distribution of Fe and Al in the soil profiles along the catena showed that leaching of solutes occurs vertically and horizontally. Although the mass balance calculations have to be considered with some caution, because they could only be related to the least weathered horizon, they nonetheless show that vertical chemical leaching is most intense on the ridge position. Along the slope (particularly well detectable in the KH3 soil profile, where several elements such as K, Na and Al show an accumulation) an increasing deplacement as solutes or in solid form (erosion and accumulation) occurs.

The vertical and lateral directions of podzolization influence not only the Al and Fe distribution, but also the fluxes of almost all major and minor elements. The open-system mass transport functions showed a high depletion of Mg and Ca in the E horizons (Fig. 4), giving rise to low concentrations of these elements in the topsoil (Table 5). The mass-fluxes were, to some extent, in relation to the local relief and slope position. The lowest Ca and Mg depletion or even occasionally an accumulation were found in the B horizons of profiles KH2 and KH3: an effect that is due to vertical leaching and lateral mass fluxes. Lateral fluxes are particularly expressed for Al (Fig. 5): a positive mass flux can be measured for KH2 and KH3 throughout the profile. Less negative elemental fluxes or even accumulation seem to be related to undulating or concave surface forms (Table 1, Figs. 4 and 5, Table 7). Negative mass fluxes of Al in upslope soils and positive fluxes along the slope are in agreement with the findings of Sommer et al. (2000; 2001) and the general principle of lateral podzolisation. This model assumes that labile Fe and Al forms (e.g.,

complexed to organic ligands) are mobilized in the upper slope section, transported by intra-layer solution flow, and accumulated along and in the lower slope section, which produces thick illuvial horizons in the lower slope.

Not only lateral solute fluxes but also erosion of solids, accumulation and mixing due to processes in slope beds (Johnson, 1993) contribute to this configuration. In addition, an aeolinan contribution could also seem to have affected the soils (this is discussed below).

The vertical distribution of primary minerals, weathering and leaching conditions determines the set of secondary phyllosilicates in the clay fraction and their differentiation along the soil profile. The dominance of illite and the lack of smectite in the clay fraction of Podzols developed from igneous and metamorphic rocks in the Sudeten Mountains has usually been explained by the high abundance of primary mica in the parent materials, the acidic conditions and the very intense chemical weathering (Bogda et al., 1998, Weber, et al., 2012). Kabala (2005) hypothesised that the predominance of illite in the E horizon is owing to two contemporary mechanisms: (1) the physical weathering of coarse feldspar minerals and the subsequent increase in low-dispersive, primary forms of this mineral in the fine silt and clay-size fractions, and (2) the chemical weathering of primary minerals under acidic conditions and the rapid leaching of the weathering products to the B horizons that resulted in a permament deficiency of alkaline cations in the E horizon giving rise to the hindrance of smectite formation. The presence of (regularly) interstratified mica-smectite, particularly at the shoulder position (KH1), indicates that low-charge expandable phases are actively formed in the soils, because interstratified mica-smectite can be considered a transition mineral between mica and smectite.

A dominant phyllosilicate in the clay fraction in the topsoil is, however, mica. The relatively high proportion might be due to passive enrichment caused by some aeolian silt input or by the above-described weathering mechanism (Kabala, 2005). Chlorite is partially dissolved or transformed (this causes, among others, a decrease in the peak at 0.72 nm; Figs. 7 and 8). The

423 influence of aeolian substrates can be inferred from the quantity of silt in the soil and its
424 mineralogical composition. The dominant minerals of aeolian silt are usually quartz (Ollier, 1969;
425 Bronger and Heinkele, 1989), mica and kaolinite. All investigated soils contain 30 – 50% silt in the
426 fine earth fraction. A particularly high silt content is detectable in soil KH3. In all investigated soils,
427 a relative increase in mica (most likely illite) in the clay fraction from the sub- to the topsoil was
428 observed. Particularly at KH3, K and Al are accumulated in the topsoil. This indicates aeolian input.
429 Aeolian material that has been eroded along the slope was probably deposited (locally) at KH3 in
430 the accumulation and mixing process zone (Fig. 12). Furthermore, all soils contain quartz, mica and
431 kaolinite throughout the profile – thus, an aeolian input seems to be likely. However, there are still
432 no convincing data about large-scale aeolian silt enrichment in the subalpine soils of the
433 Karkonosze Mts (Waroszewski et al., 2013).

434 According to Bogda and Chodak (1986), Podzols formed on gneiss or schist bedrock are
435 characterized by the presence of chlorite that may evolve into vermiculite. At least part of the
436 vermiculite is saturated with hydroxy-Al-polymers (Kabala, 2005), giving rise to the formation of
437 HIV. However, the presence of pure smectite has never been confirmed in the clay fraction of
438 Podzols in the Sudetens. Bogda et al. (1998) assumed that the low concentrations of Ca and Mg in
439 the soil solution and the preferential weathering of mica to vermiculite were the causes. Traces of
440 expandable phases may be detectable only in soils formed from fine-grained colluvial[2] materials in
441 the foot-slope zones, where the addition of an allochthonous aeolian admixure also cannot be
442 excluded (Szerszeń, 1974; Bogda et al., 1998).

443 Our investigations showed that smectites and interstratified mica-smectite minerals can be
444 present even in the eluvial horizon of Podzols, where, according to previous studies, the strong
445 leaching should promote illite formation (Bogda et al., 1998). In a next step, illite – through the

[2] fine-grained material, often having a silty loam texture, that has been moved down the slope via natural near-surface processes (e.g. erosional wash) and accumulated in concave forms of the landscape

446 release of potassium from interlayers (Bain et al., 1990; Bonifacio et al., 2009) – is transformed into
447 vermiculite. Both mica and chlorites are present in the regolith, thus providing the primary
448 substratum for the formation of smectite and interstratified mica-smectite minerals. Although not
449 clearly identifiable, it seems that some interstratified chlorite-smectite might be present (Hubert et
450 al., 2009), which would indicate an active transformation of chlorite into smectitic minerals. Egli et
451 al. (2003a) demonstrated that strong eluviation, together with the presence of organic ligands,
452 enhanced the removal of Al and enabled smectite formation (even under acidic conditions). At least
453 partially, this seems also to happen in the Podzols of the Kowarski Grzbiet. In addition, amphiboles
454 are highly susceptible to weathering (Proust et al., 2006), especially under intensive weathering and
455 acid conditions (in E horizons). They may also act as the source of smectite formation (Dreher and
456 Niederbuddee, 2000; Egli et al., 2003a). Smectites can be considered to be an end-product of
457 trioctahedral mica (Egli et al., 2008) and chlorite alteration (Righi et al., 1999) with a transition
458 product of irregularly or regularly interstratified 2:1 clay minerals (Egli et al., 2003a; Böhlert et al.,
459 2011). Interstratified mica-smectite is a transitional weathering product that may further evolve into
460 smectite, both dioctaherdal and trioctahedral (Churchmann, 1980; Wilson, 1999). Within the
461 investigated soil profiles, a transformation of trioctahedral phases to dioctahedral was discernible
462 from the subsoil to the topsoil. The decrease in trioctahedral phases (chlorite and mica) is related to
463 the increase in dioctahedral phases such as smectite and vermiculite (or even kaolinite; Fig. 10;
464 Mirabella and Egli, 2003). The highest abundance of dioctahedral species seemed to be present in
465 the soil at the ridge position (KH1).

466 Erosion, accumulation and mixing processes lead to inhomogeneous slope deposits.
467 Ultimately, these are not very favourable conditions for smectite formation. Particularly in mid-
468 slope concave positions, Al and Fe do not seem to be fully eluviated or they may even be
469 accumulated, which leads to the preservation of chloritic components (Righi et al., 1993; Carnicelli
470 et al., 1997; Egli et al., 2003b). Nonetheless, some smectite was also found in the subsoil.

Mechanical transport of clays with percolating water must be excluded, as clay coatings were found neither on ped faces nor in root channels (Table 2). In addition, the requirements for clay translocation were not present, as the soil conditions were too acidic. Thus, an in situ formation may be considered, even in the subsoil, or more likely an inheritance or accumulation from former upperslope erosion. In some cases, the B horizons contained traces of amphiboles (Table 7). The main secondary products of amphibole weathering are trioctahedral vermiculite, Fe-oxyhydroxides or smectites (Proust, 1985; Velde and Meunier, 2008). We assume that a part of the smectites in the B horizons probably developed from amphibole.

The general outline of smectite formation along the investigated slopes and profiles is given in Figure 12. Part of the smectite is inherited from the parent material and part of it is actively formed in the soils. Precursor minerals of smectite formation are chlorite and mica. Such a neo-formation seems to take place particularly at the rigde or lower slope (straight) positions. A concave topography provides less favourable conditions, because Al and Fe are not sufficiently leached away.

It is noteworthy that in all soil horizons kaolinite was detected in the clay fraction (Table 7, Fig. 11). Kaolinite slightly increased towards the E or AE horizon (cf. Fig. 11c). There may be various sources for the kaolinite: i) it is a direct transformation of mica under intensive chemical weathering conditions (Wilson, 1999, 2004); ii) the origin of the traces of kaolinite could also be traced back to the weathering of plagioclase (Egli et al., 2001b). Together with the pronounced Ca losses in the upper part of the soil profiles (Fig. 4), formation of kaolinite through weathering of plagioclase seems to be likely. Leaching conditions, in particular losses of Ca from surface horizons (Table 5), may foster feldspar weathering and kaolinite formation (Meunier and Velde, 1979). Kaolinite is not a very common component of the clay fraction of podzols. Ross (1980) noted how this is in apparent disagreement with thermodynamical equilibrium calculations, and endorsed the view that this contrast is due to the incomplete evolution and non-equilibrium of soils that, in most cases, are

geologically young and develop in rather cool climates. This would contradict the findings of several others (e.g., Weber et al, 2012) who have postulated a low present-day weathering intensity. Other possible explanations for the presence of kaolinite are: iii) aeolian deposition (Ollier, 1969; Bronger and Heinkele, 1989) and iv) inheritance from the parent material. Given that kaolinite occurs in all soil horizons, even in the parent material, at least a part of it is inherited from the Neogene regoliths (formed under subtropical conditions and advanced chemical weathering) and admixed during the slope–cover formation in the Pleistocene period (Dumanowski, 1961; Migoń and Danišík, 2012).

6. Conclusions

The slope deposits in the eastern Karkonosze Mountains showed a very complex weathering behaviour. Intensive (vertical) podzolization processes characterized by a distinct leaching of most macroelements were prevalent at the shoulder and lower slope position. Along the slope, lateral translocation of solutes also became increasingly important. In addition, aeolian deposits (illite, kaolinite) also contributed to the soil development. All this had consequences for the formation and transformation of soil minerals. In contrast to previous investigations, not only were illite- and vermiculite-type minerals recognized in the clay fraction of the Karkonosze Mountains, but so were smectites and interstratified smectite-bearing minerals. Where vertical transport processes prevailed, the geochemical conditions for smectite formation were favourable. Strong elemental leaching combined with the presence of precursor minerals such as mica and chlorite were the necessary prerequisites for smectite formation. Even along the slope, smectite was found in the subsoil. This could be due to an inheritance from the parent material or cover bed mixing processes and the accumulation of eroded upslope material.

Acknowledgement

This research was partially supported by a Sciex NMCx (nr 12.624) grant and Wroclaw University of Environemntal and Life Sciences (project nr PT/355/2014/SC). We would like to express our appreciation to Maria Budzisz-Waroszewska, Małgorzata Chilkiewicz, Janusz Kamiński and Robert Nawrocki for their assistance during field campaigns. We are furthermore indebted to Barbara Kierod and Sandra Röthlisberger for their help in the laboratory, to the authorities of the Krkonossky Narodni Park for allowing us access to the study area and to two unknown reviewers and Bruce Velde for their helpful remarks on an earlier version of this manuscript.

References

Aleksandrowski, P., Słaby, E., Szuszkiewicz, A., Galbarczyk-Gąsiorowska, L., Madej, S., Szełęg, E., 2014. Geological structure. In: Knapik R., Raj A. (Ed.) Nature of Karkonosze Mts. National Park. Karkonoski Park Narodowy, Jelenia Góra, 7-46. (in Polish)

April, R.H., Keller, D., Driscroll, C.T., 2004. Smectite in Spodosols from the Adirondac Mountains of New York. Clay Minerals 39, 99-103.

Bain, D.C., Mellor, A., Wilson, M.J., 1990. Nature and origin of an aluminous vermiculitic wethering product in acid soils from upland catchments in Scotland. Clay Minerals 25, 467-475.

Balan, E., Trocellier, P., Jupille, J., Fritsch, E., Muller, J.P., Calas, G., 2001. Surface chemistry of weathered zircons. Chem. Geol. 181, 13– 22.

Bogda, A., 1981. Minerals composition and selected properties of Cambisols derived from sudetic granitoids. Zesz.Nauk.AR Wroc., 26, pp.58. (in Polish)

545 Bogda, A., Chodak, T., Clay minerals of soils developed from gneisses. Arch. Mineralog., 41, 1,
546 303-310. (in Polish)
547 Bogda, A., Chodak, T., Szerszeń, L., 1998. Properties and composition of clay minerals in soils of
548 the Lower Silesia. AR Wrocław, pp.89. (in Polish)
549 Bonifacio, E., Falsone, G., Simonov, G., Sokolova, T., Tolpeshta, I., 2009. Pedogenic processes and
550 clay transformations in besequal soils of the Siuthern Taiga zone. Geoderma 149, 66-75.
551 Böhlert, R., Mirabella, A., Plötze, M., D., Egli, M., 2011. Landscape evolution in Val Mulix,
552 eastern Swiss Alps – soil chemical and mineralogical analyses as age proxies. Catena 87,
553 313–325.
554 Brimhall, G.H., Dietrich, W.E., 1987. Constitutive mass balance relations between chemical
555 composition, volume, density, porosity, and strain in metasomatic hydrochemical systems:
556 results on weathering and pedogenesis. Geochimica et Cosmochimica Acta 51, 567–587.
557 Bronger, A., Heinkele, T., 1989. Paleosol sequences as witnesses of Pleistocene climatic history. In:
558 Bronger, A., Catt, J.A. (Eds.), Paleopedology – Nature and Applications of Paleosols.
559 Catena Supplement 16, pp. 163-186.
560 Carnicelli, S., Mirabella, A., Cecchini, G., Sanesi, G., 1997. Weathering of chlorite to a low charge
561 expandable minerals in a spodosol on the Apennine Mountains – Italy. Clays and Clay
562 Minerals 45, 28-41.
563 Chadwick, O.A., Brimhall, G.H., Hendricks, D.M., 1990. From a black to a grey box —a mass
564 balance interpretation of pedogenensis. Geomorphology 3, 369–390.
565 Churchman, G.J., 1980. Calminerals formed from cs nd chlorites in some New Zeland soils. Clay
566 Minerals 15, 59-76.
567 Certini, G., Ugolini, F.C., Corti G., Agnelli A., 1998. Early stages of Podzolization under Corsican
568 pine (*Pinus nigra* Arn. ssp. *laurico*). Geoderma 83, 103-125.

569 Cornu, S., Lucas, Y., Lebon, E., Ambrosi, J.P., Luziao, F., Rouiller, J., Bonnay, M., Neal, C., 1999.
570 Evidence of titanium mobility in soil profiles, Manaus, central Amazonia. Geoderma 91,
571 281-295.
572 Dahms, D. Favilli, F., Krebs, R., Egli, M., 2012. Soil weathering and accumulation rates of oxalate-
573 extractable phases from alpine chronosequences of up to 1 Ma in age. Geomorphology, 151-
574 152, 99-113.
575 Dahlgren, R.A., Ugolini, F.C., 1991. Distribution and characterization of short-range-order minerals
576 in Spodosols from the Washington Cascades. Geoderma. 48,391-413.
577 Dietze, M., Kleber, A., 2010. Characterisation and prediction of thickness and material properties of
578 periglacial cover beds, Tharandter Wald, Germany. Geoderma 156, 346-356.
579 Dreher, P., Niederbudde, E.-A., 2000. Characterization of expandable layer silicates in humic –
580 ferralic cambisols (Umbrept) derived from biotite and hornblende. Journal of Plant Nutrition
581 and Soil Science 163, 447–453.
582 Dumanowski, B. 1961. Cover deposits of the Karkonosze Mts. Zeszyty Naukowe Uniwersytetu
583 Wrocławskiego, B, 8, 31-55.
584 Egli, M., Fitze, F., 2000. Formulation of pedoligicmass balance based on immobile elements: a
585 revision. Soil Science 165, 437–443.
586 Egli, M., Fitze, P., Mirabella, A., 2001. Weathering and evolution of soils formed on granitic,
587 glacial deposits: results from chronosequences of Swiss alpine environments. Catena 45, 19–
588 47.
589 Egli, M. Mirabella, A., Fitze, P. 2001b. Clay mineral formation in soils of two different
590 chronosequences in the Swiss Alps. Geoderma 104, 145-175.
591 Egli, M., Mirabella, A., Fitze, P., 2003a. Formation rates of smectites derived from two Holocene
592 chronosequences in the Swiss Alps. Geoderma 117, 81–98.

593 Egli, M., Mirabella, A., Sartori, G., Fitze, P., 2003b. Weathering rates as a function of cli mate:
594 results from a climosequence of the Val Genova (Trentino, Italian Alps). Geoderma 111, 99-
595 121.
596 Egli, M., Mirabella, A., Sartori, G. 2008. The role of climate and vegetation in weathering and clay
597 mineral formation in late Quaternary soils of the Swiss and Italian Alps. Geomorphology
598 102, 307-324.
599 Egli, M., Sartori, G., Mirabella, A., 2010. The effects of exposure and climate on the weathering of
600 late Pleistocene and Holocene Alpine soils. Geomorphology 114, 466-482.
601 Engel, Z., Nývlt, D., Křížek, M., Treml, V., Jankovská, V., Lisá, L. 2010. Sedimentary evidence of
602 landscape and climate history since the end of MIS 3 in the Krkonoše Mountains, Czech
603 Republic. Quaternary Science Reviews 29, 913-927.
604 Engel, Z., Braucher, R., Traczyk, A., Laetitia, L., ASTER team. 2014. ^{10}Be exposure age
605 chronology of the last glaciation in the Krkonoše Mountains, Central
606 Europe. Geomorphology 206, 107-121.
607 Fanning, D.S., Keramidas, V.Z., El-Desoky, M.A., 1989. Micas. In: Dixon, J.B., Weed, S.B. (eds),
608 Minerals in the Soil Environment, 2nd edition. Soil Science Society of America, Madison,
609 Wisconsin, pp. 551-634.
610 FAO, 2006. Guidelines for Soil Description, 4rd Ed. FAO, Rome.
611 Farmer, V.C., 1974. Layer silicates. In: Farmer, V.C. (Ed.), Infrared Spectra of Minerals,
612 Monograph, 4. Mineralogical Society, London, pp. 331–363.
613 Fichter, J., Turpault, M-P., Dambrine, E., Ranger, J., 1998. Mineral evolution of acid forest soils in
614 the Strengbach catchment (Vosges mountains, N-E France). Geoderma 82, 315-340.
615 Geitner, C., Schäfer, D., Bertola, S., Bussemer, S., Heinrich, K., Waroszewski J., 2014. Landscape
616 archaeological results and discussion of Mesolithic research in the Fotsch valley (Tyrol). –
617 In: Kerschner, H., Krainer, K., Spötl C. (Ed.), From the foreland to the Central Alps – Field

618 trips to selected sites of Quaternary research in the Tyrolean and Bavarian Alps (DEUQUA
619 EXCURSIONS), Berlin, pp. 106-115.
620 Hubert, F., Caner, L., Meunier, A., Lanson, B., 2009. Advances in characterization of soil clay
621 mineralogy using X-ray diffraction: from decomposition to profile fitting. European Journal
622 of Soil Science 60, 1093-1105.
623 IUSS Working Group WRB, 2014. International soil classification system for naming soils and
624 creating legends for soil maps. World Reference Base for Soil Resources 2014 World Soil
625 Resources Reports 106. FAO, Rome (181 pp.).
626 Jahn, A., 1963. Structural soils on the Czarny Grzbiet ridge and the problem of silty materials in the
627 Karkonosze Mountains. Acta Universitatis Wratislaviensis 9, 55–65. (in Polish, with English
628 abstract)
629 Jankowski, M., 2014. The evidence of lateral podzolization in sandy soils of Northern Poland.
630 Catena 112, 139–147.
631 Jäger, H., Achermann, M., Waroszewski, J., Kabala, C., Malkiewicz, M., Gärtner, H., Dahms, D.,
632 Krebs, R., Egli, M., 2015. Pre-alpine mire sediments as a mirror of erosion, soil formation
633 and landscape evolution during the last 45 ka, Catena 128, 63-79.
634 Johnson, D.L. 1993. Dynamic denudation evolution of tropical, subtropical and temperate
635 landscapes with three-tiered soils: toward a general theory of landscape evolution. –
636 Quaternary International 17, 67–78.
637 Kabala, C., 2005. Origin, properties and occurance of Podzols in different geoecological conditions
638 of the Lower Slesia. AR Wrocław, 169 pp.(in Polish with English abstract)
639 Kabala, C., Zapart, J. 2012. Initial soil development and carbon accumulation on moraines of the
640 rapidly retreating Werenskiold Glacier, SW Spitsbergen, Svalbard archipelago. Geoderma
641 175-176, 9-20.

642 Kabala, C., Waroszewski, J., Bogacz, A., Labaz, B., 2012. On the specifics of the Podzols in
643 mountains areas. Soil Science Annual. 63, 55-64.
644 Kabala, C., Bogacz, A., Łabaz, B., Szopka, K., Waroszewski, J., 2013. Diversity, dynamics and
645 threats of soils. In: Knapik R., Raj A. (Ed.) Nature of the Karkonosze National Park. Jelenia
646 Góra. 91-126. (in Polish)
647 Kacprzak, A., Derkowski, A., 2007. Cambisols developed from cover-beds in the Pieniny Mts
648 (southern Poland) and their mineral composition. Catena 71, 292–297.
649 Kitagawa, Y., 2006. Characteristics of clay minerals in Podzols and Podzolic Soils. Soil Science
650 and Plant Nutrition 51, 151-158.
651 Kleber, A., Terhorst, B., 2013. Mid-latitude slope deposits (Cover Beds). Developments in
652 Sedimentology 66. Elsevier, (302 pp.).
653 Kowaliński, S., Bogda, A., Chodak, T., 1967. Preliminary micromorphological investigations of
654 weathering products of mica in soils developed from granite in the Karkonosze Mountains.
655 Zesz.Nauk. WSR, Wrocław, 21, 66, 19-30.
656 Lanson, B., 1997. Decomposition of experimental X-ray diffraction patterns (profile fitting): a
657 convenient way to study clay minerals. Clays and Clay Mineralogy 45, 132-146.
658 Litaor, M.I., 1992. Aluminum mobility along a geochemical catena in an alpine watershed, Front
659 Range, Colorado. Catena 19:1-16.
660 Mavris, C., Egli, M., Plötze, M., Blum, J.D., Mirabella, A., Giaccai, D., Haeberli, W., 2010. Initial
661 stages of weathering and soil formation in the Morteratsch proglacial area (Upper Engadine,
662 Switzerland). Geoderma 155, 359–371.
663 Mavris, C., Plötze, M., Mirabella, A., Giaccai, D., Valboa, G., Egli, M., 2011. Clay mineral
664 evolution along a soil chronosequence in an Alpine proglacial area. Geoderma 165, 106–
665 117.

666 Mavris, C., Furrer, G., Dahms, D., Anderson, S.P., Blum, A., Goetze, J., Wells, A., Egli, M., 2015.
667 Decoding potential effects of climate and vegetation change on mineral weathering on
668 alpine soils: An experimental study in Wind River Range (Wyoming, USA). Geoderma 255-
669 256, 12-26.
670 Migoń, P., 1999. The role of preglacial relief in the development of mountain glaciation in the
671 Sudetes, with the special reference to the Karkonosze Mountains. Zeitschrift für
672 Geomorphologie, N. F., Supplement-Band 113, 33-44.
673 Migoń, P., Danišík, M., 2012. Erosional history of the Karkonosze Granite Massif–constraints from
674 adjacent sedimentary basins and thermochronology. Geological Quarterly 6(3), 440–454.
675 Migoń, P., Kacprzak, A., 2014. Lateral diversity of regolith and soils under a mountain slope —
676 implications for interpretation of hillslope materials and processes, Central Sudetes, SW
677 Poland. Geomorphology 221, 69-82.
678 Mirabella, A., Egli, M., 2003. Structural transformations of clay minerals in soils of a
679 climosequence in an Italian Alpine environment. Clays and Clay Minerals 51, 264-278.
680 Mirabella, A., Sartori, G., 1998. The effect of climate on the mineralogical properties of soils from
681 Val Genova valley – Trentino, Italy. Fresenius Environmental Bulletin 7 (5a-6a). 478-483.
682 Mirabella, A., Egli, M., Carnicelli, S., Sartori, G. 2002. Influence of parent material on clay
683 minerals in podzols of Trentino – Italy. Clay Minerals, 37, 699-707.
684 Mourier, B., Poulenard, J., Carcaillet, C.,Williamson, D., 2010. Soil evolution and subalpine
685 ecosystem changes in the French Alps inferred from geochemical analysis of lacustrine
686 sediments. J. Paleolimnol. 44, 571–587.
687 Moore, D.M., Reynolds, R.C., 1997. X-ray Diffraction and the Identification and Analysis of Clay
688 Minerals, 2nd ed. Oxford Univ. Press, New York.
689 Nemecek, J., 2001. Taxonomicky klasifikacni system pud Ceske republiki. Academia, Praha, aa.
690 156. (in Czech)

691 Ollier, C.D., 1969. Weathering. Oliver & Boyd, Edinburgh, Scotland.
692 Proust, D., 1985. Amphibole weathering in a glucophane-schist (Ile de Groix, Morbihan, France).
693 Clay Minerals 20, 161-170.
694 Proust, D., Caillaud, J., Fontaine, C., 2006. Clay minerals in early amphibole weathering: tri- to
695 dioctahedral sequence as a function of crystallization sites in the amphibole. Clays and Clay
696 Minerals 54, 351-362.
697 Reynolds, R.C., 1972. Clay minerals formation in an alpine environment. Clays and Clay Minerals
698 19, 361-374.
699 Righi, D., Petit, S., Bouchet, A., 1993. Characterization of hydroxy-interlayered vermiculite and
700 illite-smectite interstratified minerals from weathering of chlorite in a Cryorthod. Clays and
701 Clay Minerals 41, 484-495.
702 Righi, D., Huber, K., Keller, C., 1999. Clay formation and podzol development from postglacial
703 moraines in Switzerland. Clay Minerals 34, 319-322.
704 Ross, G.J., 1980. The mineralogy of Spodosols. In: Theng, B.K.G. (Ed.), Soils with Variable
705 Charge. Soil Bureau, Department of Scientific and Industrial Research, Lower Hutt, New
706 Zealand, pp. 127–143.
707 Senesi, N., D'Orazio, V., Ricca, D., 2003. Humic acids in the first generation of EUROSOILS.
708 Geoderma 116, 325-344.
709 Senkayi, A.L., Dixon J.B., Hossner J.R., 1981. Transformation of chlorite to smectite through
710 regularly interstratified intermediates. Soil Science Society of America Journal 45, 650-656.
711 Skiba, M., Szczerba, M., Skiba, S., Bish, D.L., Grybos, M., 2011. The nature of interlayering in
712 clays from a podzol (Spodosol) from theTatra Mountains, Poland. Geoderma 160, 425-433.
713 Sobik, M., Błaś, M., Migała, K., Godek, M., Nasiółkowski, T., 2013. Climate. In: Knapik R., Raj A.
714 (Ed.) Nature of Karkonosze Mts. National Park. Karkonoski Park Narodowy, Jelenia Góra,
715 147-187. (in Polish)

716 Sommer, M., Halm, D., Weller, U., Zarei, M., Stahr, K., 2000. Lateral Podzolization in a granite
717 landscape. Soil Sci. Soc. Am. J. 64, 1434-1442.
718 Sommer, M., Halm, D., Geisinger, C., Andruschkewitsch, I., Zarei, M., Stahr, K., 2001. Lateral
719 podzolization in a sandstone catchment. Geodema 103, 231-247.
720 Stevenson, F.J., 1994. Humus Chemistry: Genesis, Composition, Reactions, 2nd ed. Wiley, New
721 York.
722 Stiles, C.A., Mora, C.I., Driesse, S.G., 2003. Pedogenetic processes and domain boundaries in a
723 Vertisol climosequence: evidence from titanium and zirconium distribution and
724 morphology. Geoderma 116, 279–299
725 Szerszeń, L., 1974. Influence of bioclimatic conditions on pedogenesis in soils of Sudetes
726 Mountains and Spitsbergen. Soil Science Annual 25, 53-99.
727 Tomita, K., 1977. Experimental transformation of 2M sericite into a rectorite-type mixed-layer
728 mineral by treatment with various salts. Clays and Clay Minerals 25, 302-308.
729 Traczyk, A., Migoń, P., 2000. Cold-climate landform patterns in the Sudetes. Effects of lithology,
730 relief and glacial history. Acta Universitatis Carolinae 35, 185–210.
731 Ugolini, F.C., Dahlgren, R.A., 1991. Weathering environments and occurrence of
732 imogolite/alophane in selected andisols and spodosols. Soil Sci. Soc. Am. J. 55, 1166-1171.
733 Van Reeuwijk, L.P., 2002. Procedures for Soil Analysis, 6th ed. ISRIC, Wageningen, Netherlands.
734 Velde, B., Meunier A., 2008. The origin of clay minerals in soils and weathered rocks. Springer,
735 Berlin. 403 pp.
736 Viennet, J.,C., Hubert, F., Ferrage, E., Tertre, E., Legout, A.,, Turpault, M.,P., 2015. Investigation
737 of clay mineralogy in a temperate acidic soil of a forest using X-ray diffraction profile
738 modeling: Beyond the HIS and HIV description. Geoderma 241-242, 75-86.
739 Wada, K., 1989. Allophane and imogolite. In: Dixon J.B. Weed S.B., (Eds.) Minerals in Soil
740 Environments, 2nd ed. Soil Science Society of America, Madison, WI, pp. 1051-1087.

741 Waroszewski, J., Kabała, C., Turska, A. 2010. Specific properties of soils on the Kowarski Grzbiet
742 Ridge in the Karkonosze Mts. Opera Corcontica 47/2010 Suppl. 1, pp. 47-56. (in Polish with
743 English abstract)
744 Waroszewski, J., Kalinski, K., Malkiewicz, M., Mazurek, R., Kozlowski, G., Kabala, C. 2013.
745 Pleistocene–Holocene cover-beds on granite regolith as parent material for Podzols — An
746 example from the Sudeten Mountains. Catena 104, 161-173.
747 Waroszewski, J., Malkiewicz, M., Mazurek, R., Labaz, B., Jezierski, P., Kabala, C., 2015a.
748 Lithological discontinuities in Podzols developed from sandstone cover beds in the Stolowe
749 Mountains (Poland). Catena 126, 11-19.
750 Waroszewski, J., Kabala, C., Jezierski, P., 2015b. Relief-induced soil differentiation at the
751 sandstone-mudstone contact in the Stołowe Mountains, SW Poland. Zeitschrift für
752 Geomorphologie 59, Suppl.1, 211-226.
753 Weber, J., Tyszka, R., Kocowicz, A., Szadorski, J., Debicka, M., Jamroz, E., 2012. Mineralogical
754 composition of clay fraction of soils derived from granitoids of the Sudetes and Fore-Sudetic
755 Block, SW Poland. European Journal of Soil Science 63, 762–772.
756 White, A.F., 1995. Chemical weathering rates of silicate minerals in soils. In: White, A.F., Brantley,
757 S.L. (Eds.), Chemical Waethering Rates of Silicate Minerals. Reviews in Mineralogy, vol.
758 31, Mineralogical Society of America, pp. 407–461.
759 Wilson, M.J., 1999. The origin and formation of clay minerals in soils: past, present and future
760 perspectives. Clay Minerals 34, 7-25.
761 Wilson, M.J., 2004. Weathering of the primary rock-forming minerals: processes, products and
762 rates. Clay Minerals 39, 233-266.
763

Table
Click here to download Table: 7_Table_1.docx

Table 1. General characteristic of sampling sites

Profile	Elevation (m a.s.l.)	Slope aspect (°)	Slope position	Slope shape (curvature)	Vegetation	Soil classification (IUSS Working Group WRB 2014)
KH1	1268	5	upper slope (shoulder)	convex	*Vaccinio-Piceetea*	Skeletic Albic Folic Podzol (Loamic)
KH2	1258	15	middle slope (back slope)	straight/concave	*Vaccinio-Piceetea*	Skeletic Albic Histic Podzol (Loamic)
KH3	1215	10	middle slope (back slope)	concave	*Vaccinio-Piceetea*	Alumic Skeletic Histic Cambisol (Siltic)
KH4	1142	15	lower slope (footslope)	straight	*Vaccinio-Piceetea*	Skeletic Albic Folic Podzol (Loamic)

Table
Click here to download Table: 8_Table_2.docx

Table 2. Morphological features of the soil profiles

Profile	Soil horizon	Depth (cm)	Colour (moist)	Rock fragments	Structure	Consistency (moist)	Boundary
KH1	O	10-0	10YR 2/2	C			
	E	0-7	10YR 5/1	M	SB, MO	FR	C, W
	Bhs	7-25	7.5YR 4-5/6	A	SB, WE	FR	C
	Bs	25-60	2.5 Y 5/6	A	AS/PL, WE	FR	G
	BC	60+	2.5Y 6/6	D	AS-PL, WE	FR/FI	
KH2	O	12-0	10YR 2/1	C			A/C, W
	E	0-18	10YR 5/2-3	A	SB, MO	FR	C
	Bhs	18-30	10YR 4/6	A	SB, WE	FR	G
	Bs	30-45	10YR 6/8	A	AS/PL, WE	FI	G
	BC	45-60	2.5Y 5/6	D	AS/PL, MO	FI/FR	
KH3	O	10-0	10YR 2/1	F			A/C, W
	AE	0-5	10YR 5/2	M	AB, MO	FR	G
	Bh	5-30	7.5YR 3/2	A	SB, WE	FR	C
	Bs	30-55	7.5YR 4/6	A	AS, WE/MO	FI	G
	BC	55-70	10YR 5/6	D	AS/PL, MO	FI/FR	
KH4	O	12-0	7.5YR 3/1				C, W
	E	0-10	7.5YR 5/2	M	AB, MO	FR	G
	Bh	10-20	7.5YR 3/3	A	AS, MO	FR	G
	Bhs	20-40	10YR 3/4	A	AS/PL, MO	FR/FI	G
	BC	40-60	10YR 4/6	A	AS,MO	FR/FI	

Explanations: abundance of rock fragments: V - very few (0–2%), F - few (2–5%), C - common (5–15%), M - many (15–40%), A - abundant (40–80%), D - dominant (>80%); types of soil structure: AB - angular blocky, AS - angular blocky, SB - subangular blocky, PL ¬ platy; grade of development: WE - weak, MO - moderate,; consistency (moist): FR — friable, FI — firm; horizon boundary (distinctness, topography): A - abrupt, C - clear, G - gradual, W - wavy.

Table
Click here to download Table: 9_Table_3.docx

Table 3. Typical physical and chemical properties of the investigated soils

Soil Horizon	Depth (cm)	Bd	pH	$C_{org.}$	Ex. Aci.	BC	Fe_o	Fe_d	Al_o	Al_d	Fe_o/Fe_d	$Al_o+1/2Fe_o$
		g cm^{-3}	KCl	%	cmol·$(kg)^{-1}$		%					%
Profile KH1 - Skeletic Albic Folic Podzol (Loamic)												
O	10-0	-	2.60	22.5	3.24	4.07	-	-	-	-	-	-
E	0-7	0.83	3.09	2.18	5.56	1.68	0.23	0.31	0.05	0.06	0.75	0.23
Bhs	7-25	1.20	3.52	3.48	3.36	1.33	3.31	3.74	0.33	0.46	0.89	3.31
Bs	25-60	1.39	4.31	0.60	7.80	0.59	2.47	2.65	0.37	0.51	0.93	2.47
Profile KH2 - Skeletic Albic Histic Podzol (Loamic)												
O	12-0		2.83	15.3	9.52	4.91	-	-	-	-	-	-
E	0-18	1.04	3.47	2.35	5.44	1.02	0.67	0.77	0.10	0.46	0.88	0.44
Bhs	18-30	1.11	3.63	1.83	7.48	1.12	2.09	2.47	0.29	0.34	0.85	1.35
Bs	30-45	1.27	3.86	0.99	5.28	0.73	0.79	1.22	0.19	0.23	0.65	0.60
BC	45-60	1.39	4.08	0.62	4.52	0.68	0.47	0.92	0.20	0.24	0.52	0.44
Profile KH3 - Alumic Skeletic Histic Cambisol (Siltic)												
O	10-0	-	3.20	30.9	7.64	7.12	-	-	-	-	-	-
AE	0-5	0.67	3.56	9.11	11.1	3.84	1.89	1.95	0.33	0.49	0.97	1.28
Bh	5-30	0.90	3.71	6.14	9.12	1.86	1.74	1.81	0.38	0.54	0.96	1.25
Bs	30-55	0.70	4.10	2.37	4.76	1.06	2.66	2.96	0.81	0.91	0.90	2.15
BC	55-70	1.11	4.32	0.95	2.88	0.87	1.50	1.97	0.51	0.58	0.76	1.27
Profile KH4 - Skeletic Albic Folic Podzol (Loamic)												
O	12-0	-	3.05	34.2	6.92	5.93	-	-	-	-	-	-
E	0-10	0.83	3.11	2.62	5.36	0.68	0.23	0.31	0.06	0.08	0.73	0.18
Bh	10-20	0.90	3.40	4.52	9.96	0.60	2.66	2.72	0.26	0.35	0.97	1.59
Bhs	20-40	0.87	3.70	3.09	7.52	0.59	2.02	2.36	0.34	0.49	0.86	1.35
BC	40-60	1.01	4.05	2.12	5.24	0.42	2.07	2.68	0.51	0.60	0.77	1.55

Explanations: Bd — bulk density, $C_{org.}$ — organic carbon, BC — sum of exchangeable base cations, Ex. Aci. — exchangeable acidity, Fe_d, Al_d — dithionite iron and aluminum, Fe_o, Al_o — oxalate iron and aluminum, Fe_o/Fe_d — iron activity index, $Al_o+1/2Fe_o$ — illuviation (podzolization) index.

Table
Click here to download Table: 10_Table_4.docx

Table 4. Particle size distribution of the investigated soils

Soil horizon	Depth [cm]	Skeleton content	Sand					Silt		Clay fraction	Sum of fractions		Texture class
			vcS	cS	mS	fS	vfS	cSi	fSi		Sand	Silt	
		%											
Profile KH1 - Skeletic Albic Folic Podzol (Loamic)													
E	0-7	10	3	9	10	15	12	20	27	4	49	47	SL
Bhs	7-25	50	3	7	9	19	14	25	19	4	52	44	SL
Bs	25-60	80	6	7	8	14	12	24	23	6	47	47	SL
Profile KH2 - Skeletic Albic Histic Podzol (Loamic)													
E	0-18	50	4	7	9	17	11	23	23	6	48	46	SL
Bhs	18-30	70	5	5	7	13	16	26	24	4	46	50	SiL
Bs	30-45	70	4	5	6	10	17	25	23	10	42	48	SL
BC	45-60	80	4	5	6	12	13	33	17	10	40	50	SiL
Profile KH3 - Alumic Skeletic Histic Cambisol (Siltic)													
AE	0-5	30	2	3	4	9	10	22	46	4	28	68	SiL
Bh	5-30	80	5	8	10	14	11	22	28	2	48	50	SiL
Bs	30-55	80	5	5	7	21	13	30	16	3	51	46	SL
BC	55-70	90	4	7	10	18	19	23	15	4	58	38	SL
Profile KH4 - Skeletic Albic Folic Podzol (Loamic)													
E	0-10	40	5	9	9	19	16	18	20	4	58	38	SL
Bh	10-20	50	3	6	14	22	19	16	16	4	64	32	SL
Bhs	20-40	50	7	7	9	21	19	16	17	4	63	33	SL
BC	40-60	50	8	6	9	25	20	14	12	6	68	26	SL

Textural classes: SL—sandy loam, SiL —silt loam; fine-earth fractions (<2 mm):vcS—very coarse sand, cS—coarse sand, mS —medium sand, fS— fine sand, vfS — very fine sand, cSi — coarse silt, fSi — fine silt.

Table

Click here to download Table: 11_Table_5.docx

Table 5. Major element contents in the fine earth fraction

Horizon	Depth	Na_2O	MgO	K_2O	CaO	Al_2O_3	Fe_2O_3	SiO_2	P_2O_5	MnO	TiO_2	(K+Ca)/Ti
	cm	%										
Profile KH1 - Skeletic Albic Folic Podzol (Loamic)												
E	0-7	1,28	0,85	4,51	0,07	17,75	2,13	67,33	0,026	0,029	1,140	6,79
Bhs	7-25	0,99	1,20	2,88	0,13	13,39	10,75	50,68	0,166	0,058	0,855	5,92
Bs	25-60	1,16	1,65	3,68	0,22	16,19	6,13	65,42	0,050	0,092	0,989	6,62
Profile KH2 - Skeletic Albic Histic Podzol (Loamic)												
E	0-18	0,99	0,88	3,63	0,07	14,52	2,76	67,24	0,105	0,020	1,048	5,97
Bhs	18-30	0,88	1,43	2,93	0,18	12,89	7,48	61,76	0,100	0,044	0,895	5,84
Bs	30-45	0,99	1,47	3,01	0,25	12,72	5,39	68,35	0,042	0,056	0,965	5,65
BC	45-60	1,10	1,47	3,08	0,27	12,70	4,97	71,18	0,016	0,058	1,011	5,54
Profile KH3 - Alumic Skeletic Histic Cambisol (Siltic)												
AE	0-5	1,18	1,12	4,23	0,11	18,34	4,91	45,93	0,422	0,010	0,759	9,64
Bh	5-30	1,05	1,17	3,84	0,06	17,67	5,17	52,65	0,406	0,015	0,865	7,64
Bs	30-55	0,95	1,35	2,68	0,14	14,55	8,24	52,11	0,196	0,029	0,781	6,08
BC	55-70	1,13	1,71	3,20	0,15	16,00	6,63	58,79	0,134	0,050	0,944	5,98
Profile KH4 - Skeletic Albic Folic Podzol (Loamic)												
E	0-10	1,16	0,77	3,14	0,11	13,29	1,97	72,74	0,054	0,020	1,094	5,01
Bh	10-20	1,04	0,93	2,53	0,15	12,04	6,32	57,51	0,148	0,022	0,970	4,64
Bhs	20-40	1,04	0,98	2,45	0,19	11,55	6,26	61,76	0,109	0,025	0,985	4,50
Bs	40-60	1,05	1,47	2,58	0,25	13,82	7,43	58,19	0,125	0,038	0,970	4,87

Table
Click here to download Table: 12_Table_6.docx

Table 6. Relative elemental losses for Si, P and Mn (open-system mass transport function $\tau_{j,w}$)

Horizon	Depth (cm)	Si	P	Mn
Profile KH1 - Skeletic Albic Folic Podzol (Loamic)				
E	0-7	-0,10	-0,55	-0,73
Bhs	7-25	-0,10	2,86	-0,27
Bs	25-60	0	0	0
Profile KH2 - Skeletic Albic Histic Podzol (Loamic)				
E	0-18	-0,08	5,22	-0,66
Bhs	18-30	-0,01	5,93	-0,14
Bs	30-45	0,01	1,70	0,02
BC	45-60	0	0	0
Profile KH3 - Alumic Skeletic Histic Cambisol (Siltic)				
AE	0-5	-0,03	2,92	-0,74
Bh	5-30	-0,02	2,31	-0,66
Bs	30-55	0,07	0,77	-0,30
BC	55-70	0	0	0
Profile KH4 - Skeletic Albic Folic Podzol (Loamic)				
E	0-10	0,11	-0,62	-0,53
Bh	10-20	-0,01	0,18	-0,41
Bhs	20-40	0,05	-0,14	-0,33
Bs	40-60	0	0	0

Table
Click here to download Table: 13_Table_7.docx

Table 7. Mineral composition of the clay fraction (< 2 μm)

Soil profile	Soil horizon	Quartz	Mica	Chlorite	Kaolinite	Smectite	Interstratified mica-smectite	Interstratified mica-vermiculite (or HIV)	Vermiculite	Amphibole
KH1	E	++	++	-	+	(+)	+	(+)	+	-
	Bhs	++	++	(+)	+	(+)	-	+	(+)	-
	Bs	++	++	-	+	(+)	-	+	(+)	(+)
KH2	E	++	++	(+)	+	+	(+)	(+)	+	-
	Bhs	++	++	+	+	+	-	+	(+)	-
	Bs	++	++	+	+	+	-	+	(+)	-
	BC	++	++	+	+	+	-	+	(+)	(+)
KH3	AE	++	++	(+)	+	(+)	-	+	+	-
	Bh	++	++	(+)	+	+	-	+	(+)	-
	Bs	++	++	+	+	(+)	-	+	(+)	-
	BC	++	++	+	+	(+)	-	+	(+)	(+)
KH4	E	++	++	-	+	+	(+)	+	+	-
	Bh	++	++	+	+	(+)	-	+	(+)	-
	Bhs	++	++	+	+	(+)	-	+	(+)	-
	Bs	++	++	+	+	(+)	-	+	(+)	(+)

++ major, + minor, (+) trace, - absent

Figure captions (if not provided in the manuscript)
Click here to download Figure captions (if not provided in the manuscript): 26_Figure_captions.docx

Figure captions

Fig. 1. Southern slopes of Skalny Stół (Kowarski Grzbiet/ Střeha) with the investigated soil profiles (KH 1-4) along a catena (view from Czarna Kopa).

Fig. 2. Soils along the studied toposequence.

Fig. 3. Rock thin sections: quartzite (a - PPL) and mica schist (b- XPL, c -PPL ,d -XPL). The individual minerals are: Qz - quartz, Ms - muscovite, Chl - chlorite, Grt - garnet, Tur – tourmaline.

Fig. 4. Open-system mass transport function (τ) for Na, Ca, K, Mg along the soil profiles.

Fig. 5. Open-system mass transport function (τ) for Fe and Al along the soil profiles.

Fig. 6. XRD pattern of the randomly-oriented powder mounts (profile KH1).

Fig. 7. XRD patterns of soil clays (< 2 μm) of the Eg and BC horizon of profile KH2. The XRD curves are corrected for Lorentz and polarization factors; *d*-spacings are given in nm. EG = ethylene glycol solvation, Mg = Mg-saturation, K = K-saturation and corresponding heating treatments.

Fig. 8. XRD patterns of the EG-solvated clay fraction from the topsoils along the toposequence. The measured values (squares), modelled elementary curves and the modelled overall curve are shown. The XRD curves are corrected for Lorentz and polarization factors; *d*-spacings are given in nm.

Fig. 9. XRD patterns of the EG-solvated clay fraction from the subsoils (B and BC horizon) along the toposequence. The measured values (squares), modelled elementary curves and the modelled overall curve are shown. The XRD curves are corrected for Lorentz and polarization factors; *d*-spacings are given in nm.

Fig. 10. XRD patterns in the d_{060} region of the soil clays from the investigated sites (topsoil and subsoil). The peak range between 0.1560 and 0.1530 nm was assigned to trioctahedral and the one between 0.1530 and 0.1490 to dioctahedral phases. Given are the measured values (squares), modelled elementary curves and the modelled overall curve.

Fig.11. DRIFT spectra of selected soil samples (clay fraction): a – horizons of profile KH3; b – AE and E horizons of all soils along the catena; c – Normalised (min-max method) IR spectra of soil clays in the OH-stretching region 4000–3000 cm^{-1}.

Fig. 12. Scheme of presumed weathering and mineral transformation processes in the soil profiles and along the slope. Measurable processes are given by solid lines and presumed processes by dashed lines.

Figure

Click here to download high resolution image

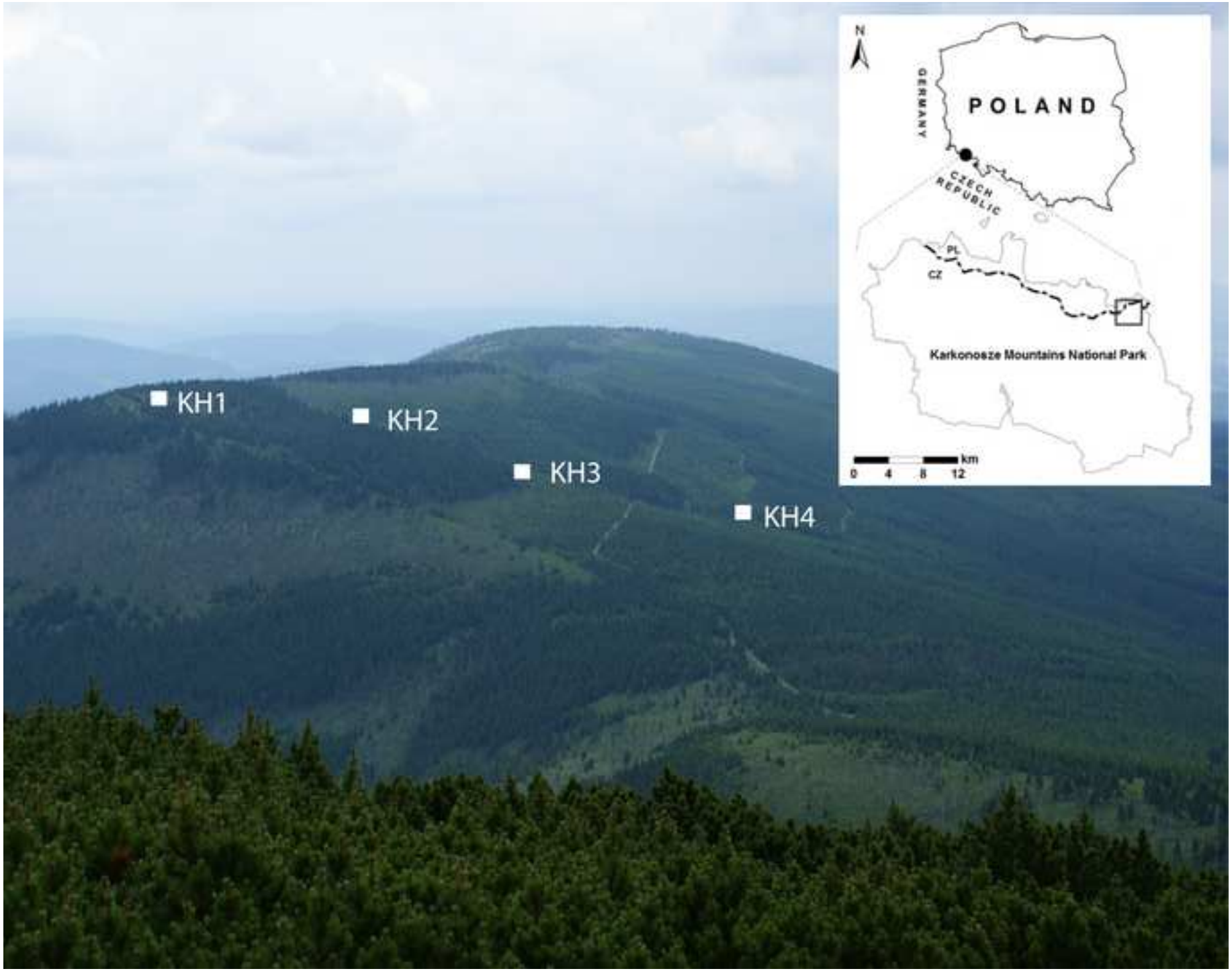

Figure

Click here to download high resolution image

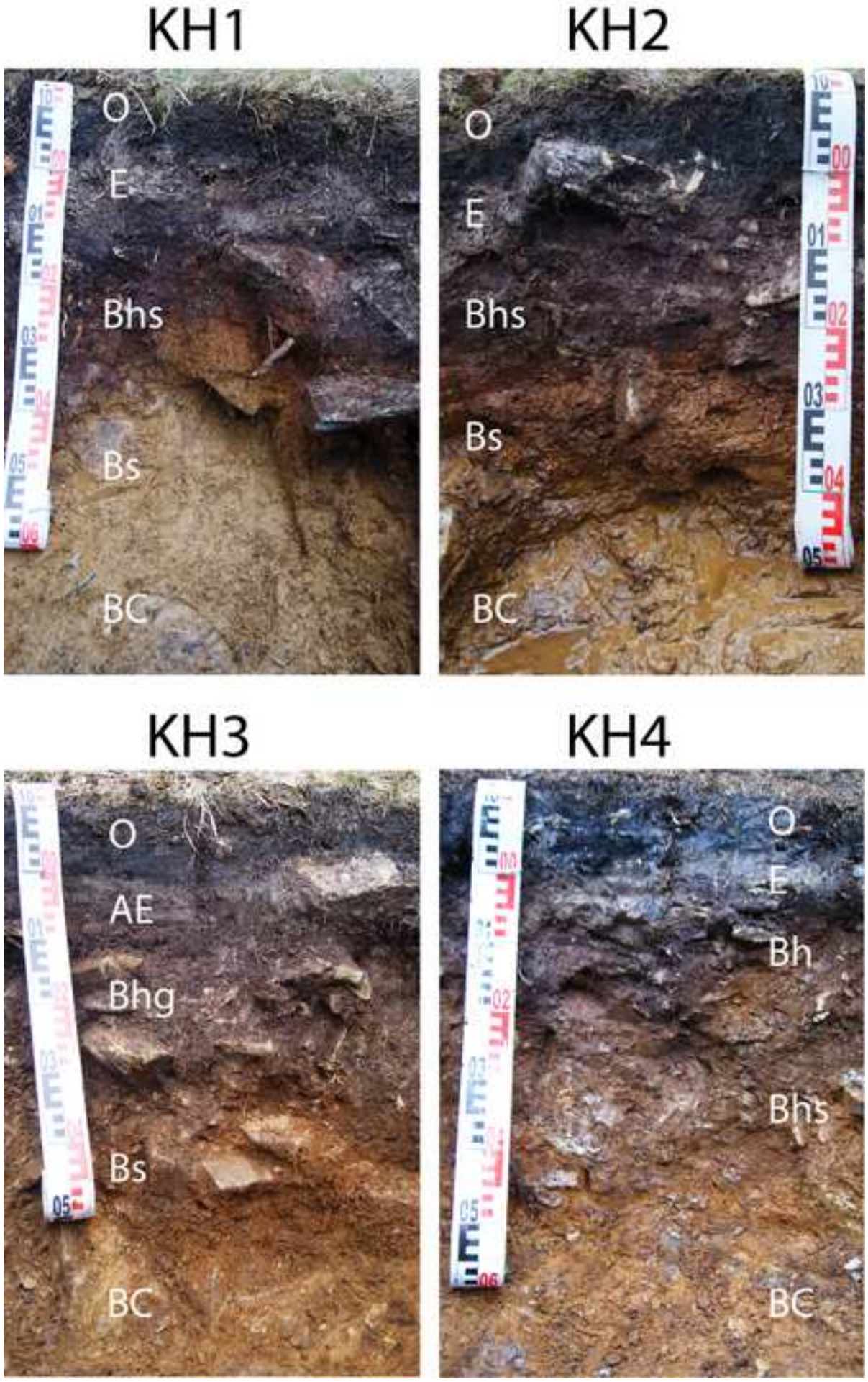

Figure

Click here to download high resolution image

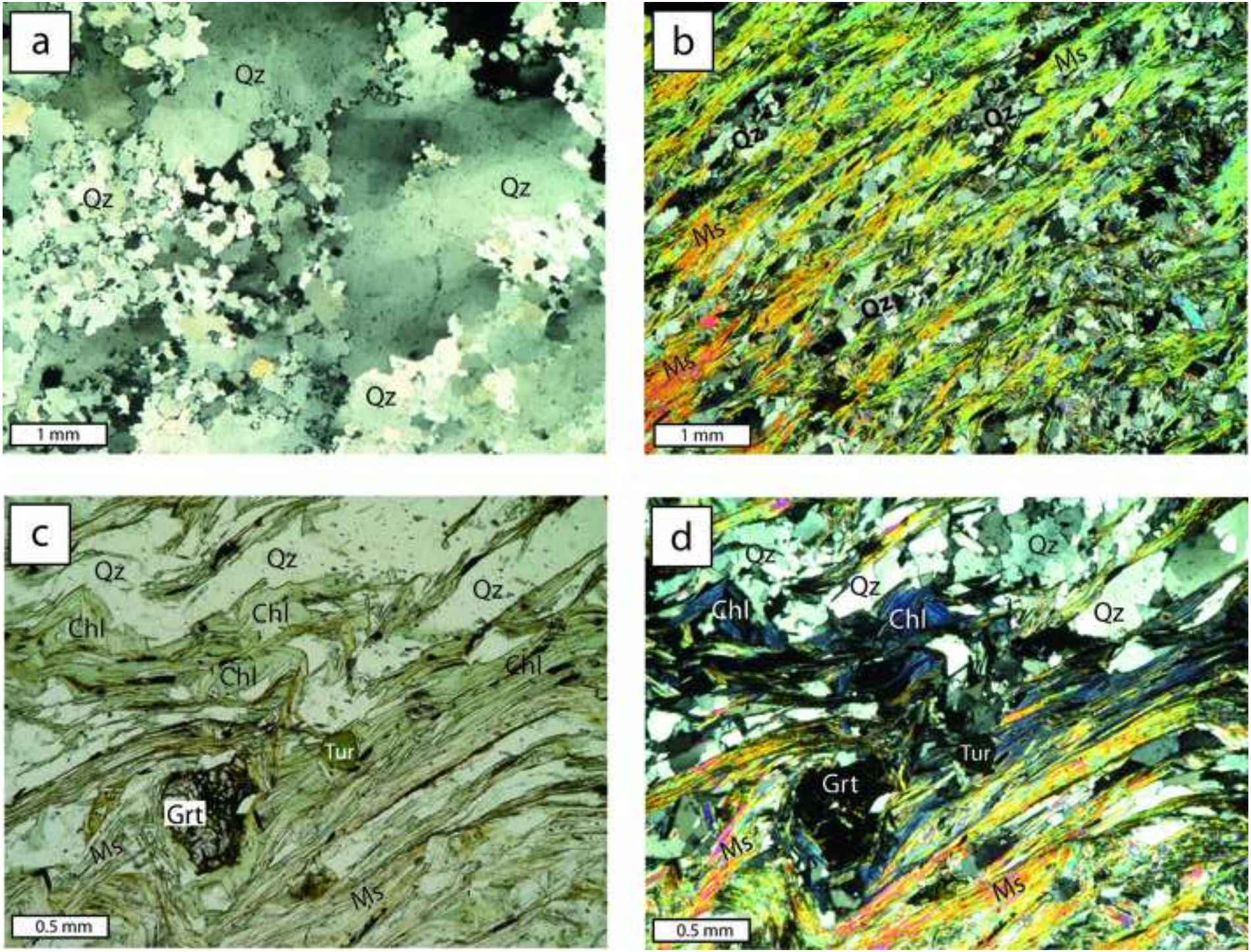

Figure

Click here to download high resolution image

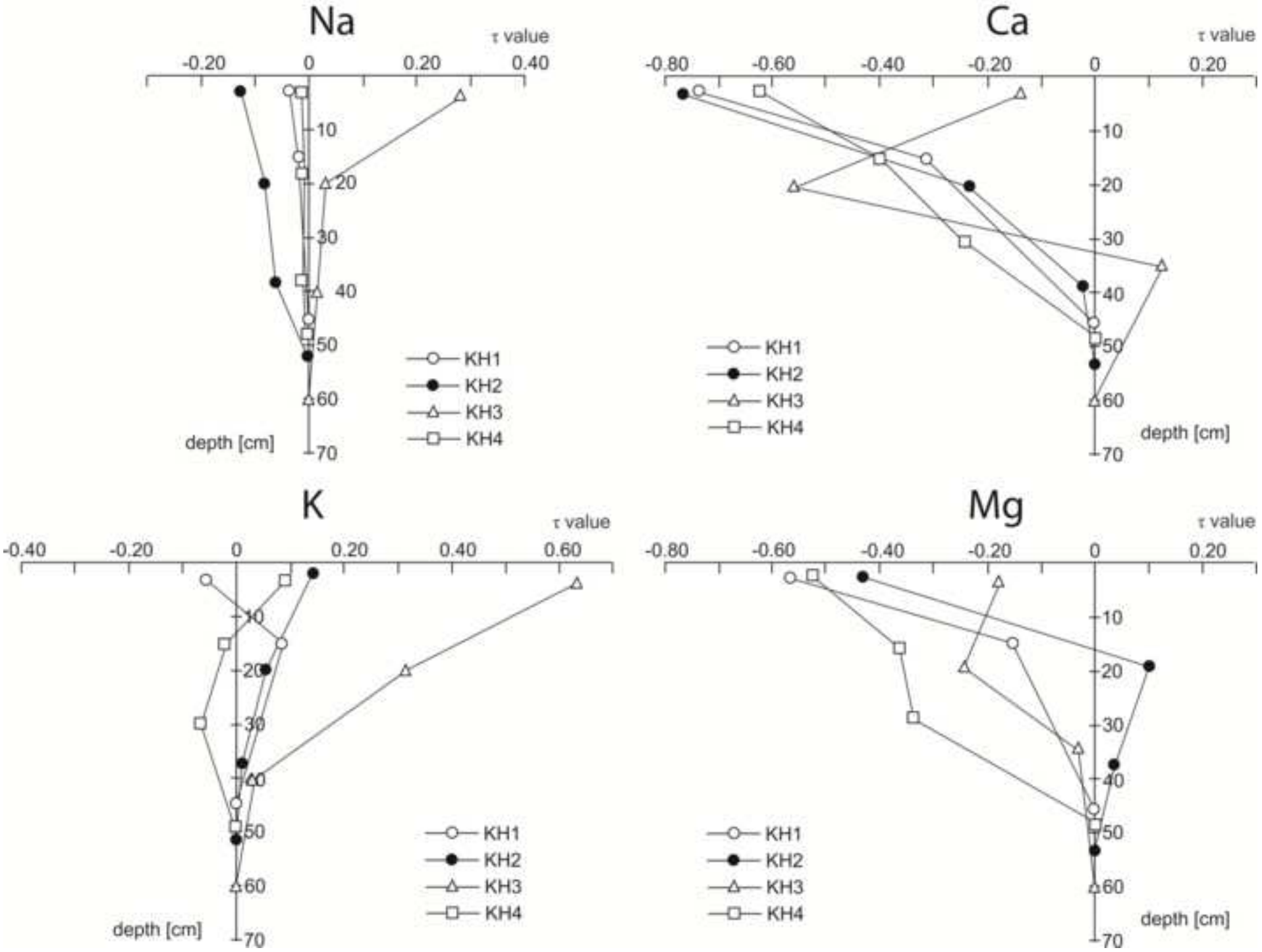

Figure
Click here to download high resolution image

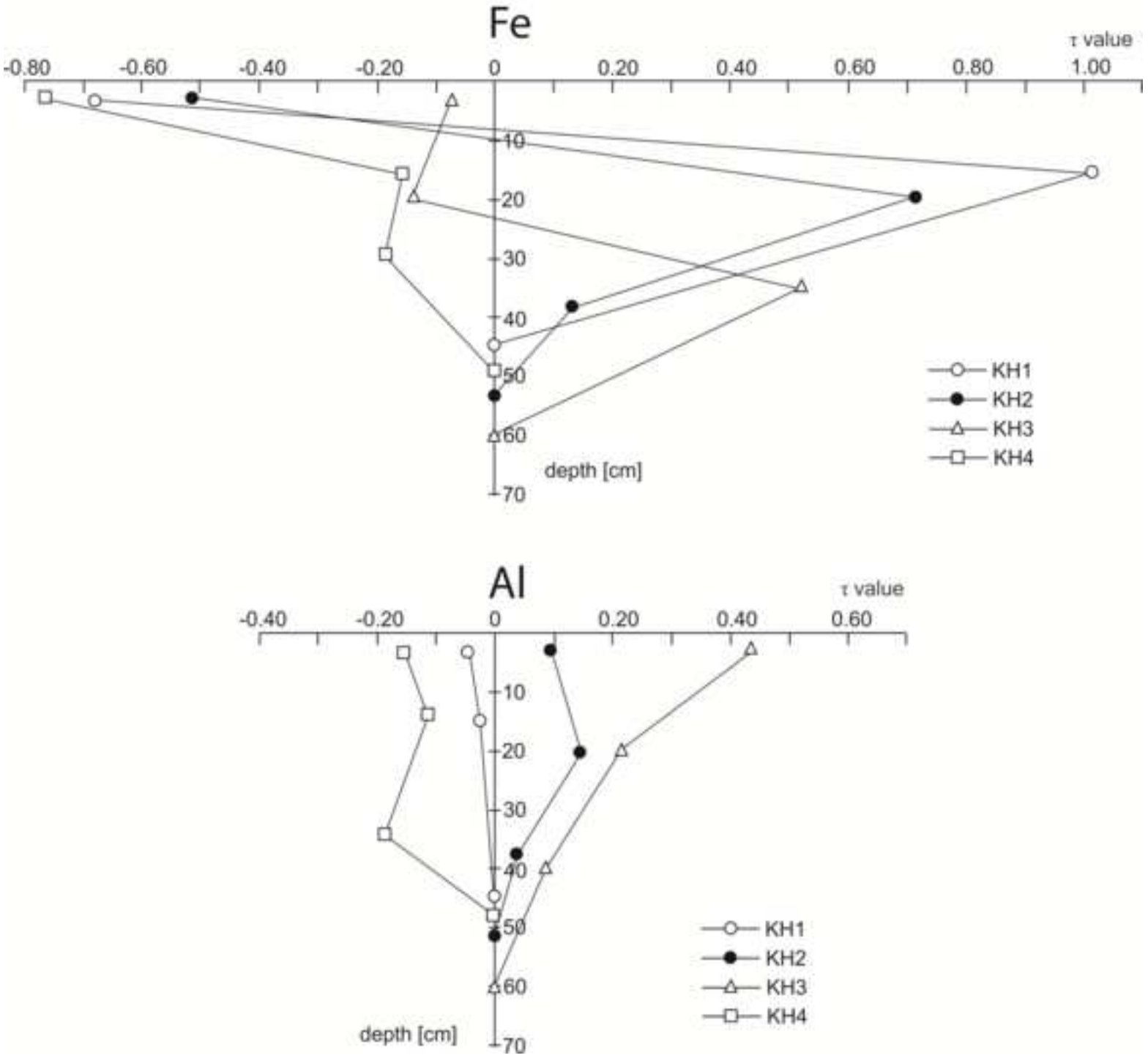

Figure

Click here to download high resolution image

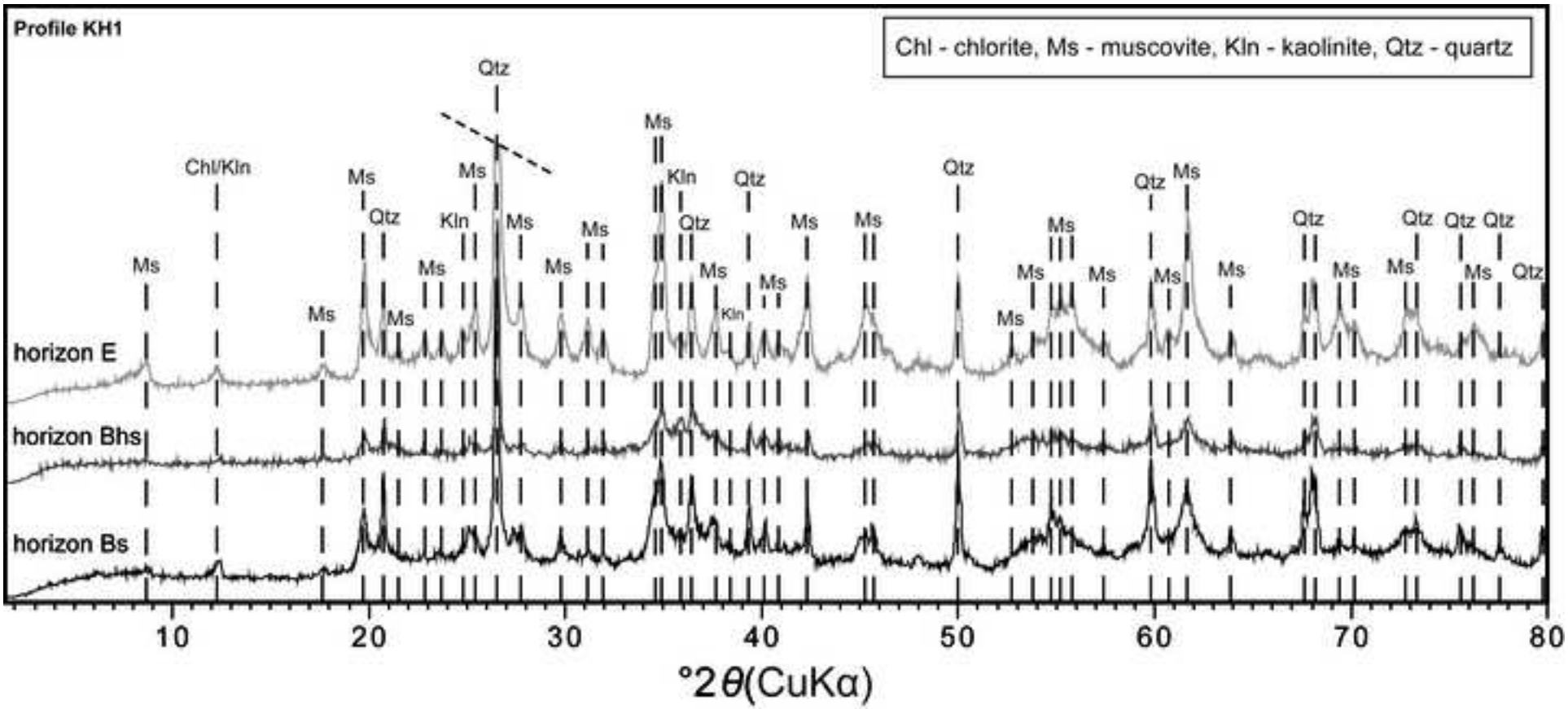

Figure
Click here to download high resolution image

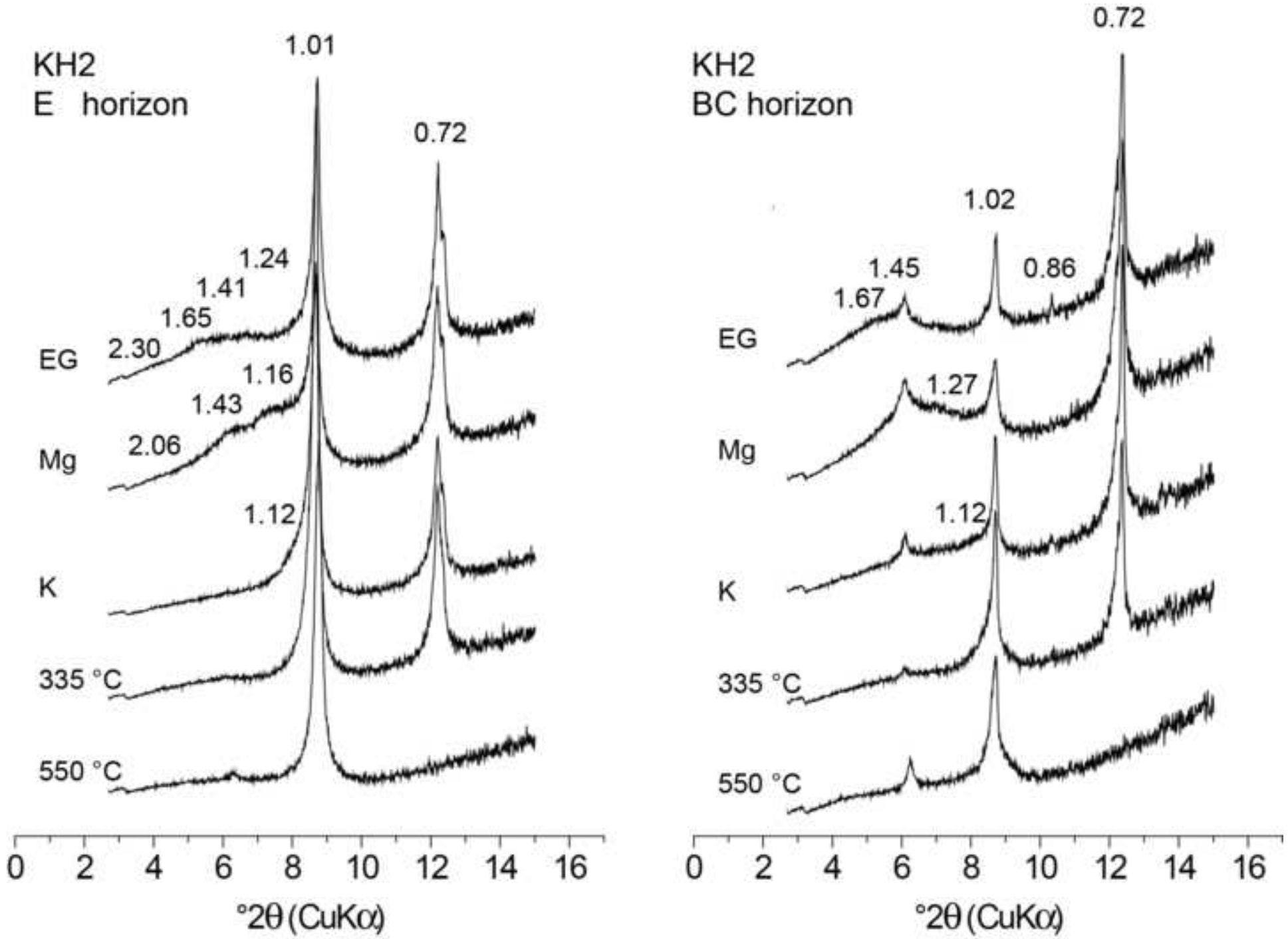

Figure

Click here to download high resolution image

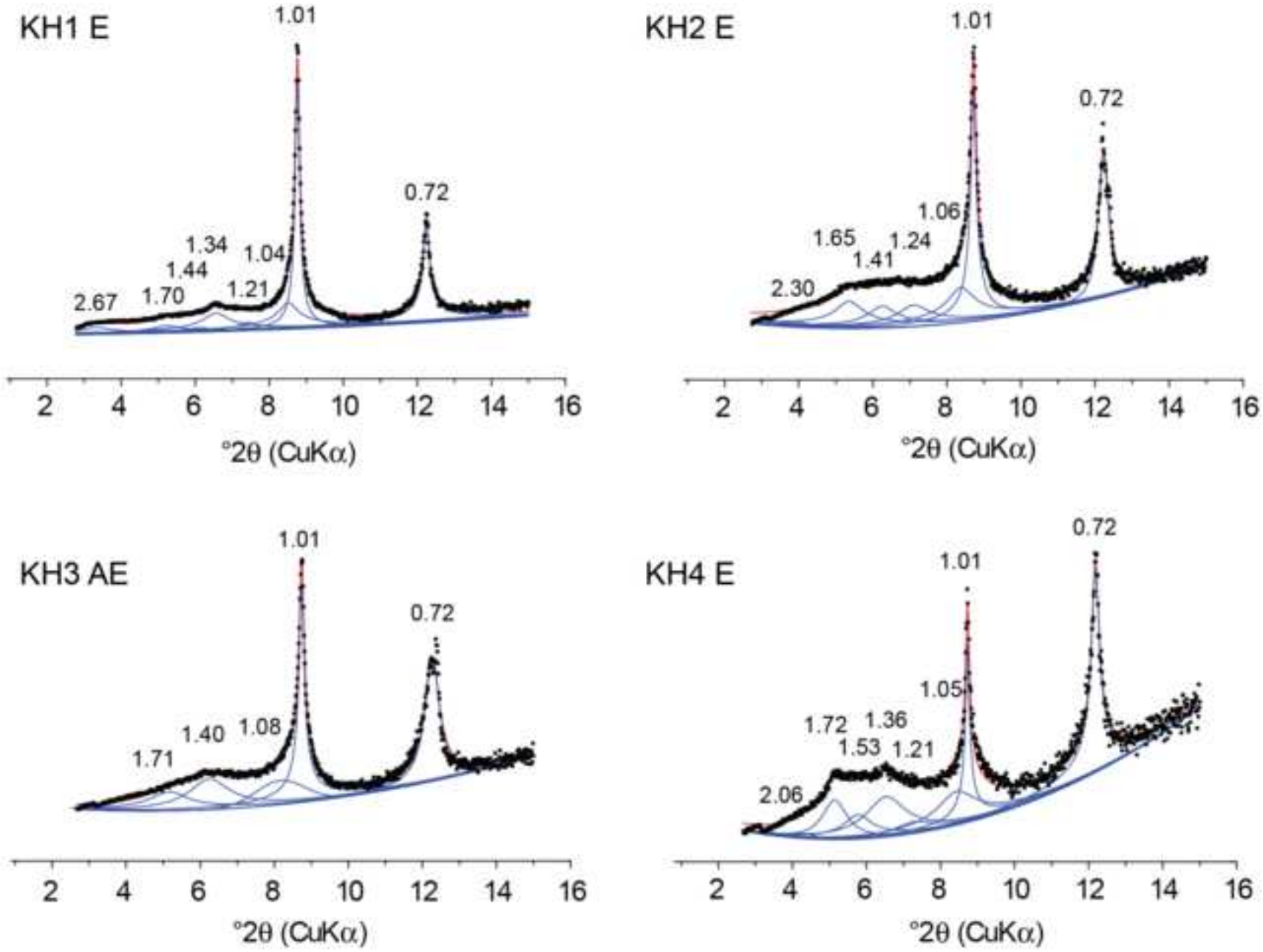

Figure
Click here to download high resolution image

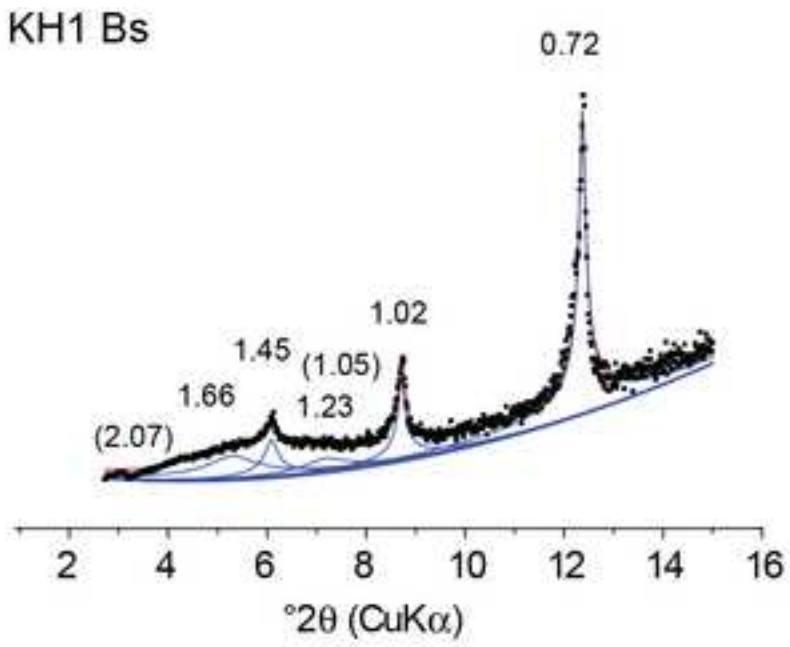

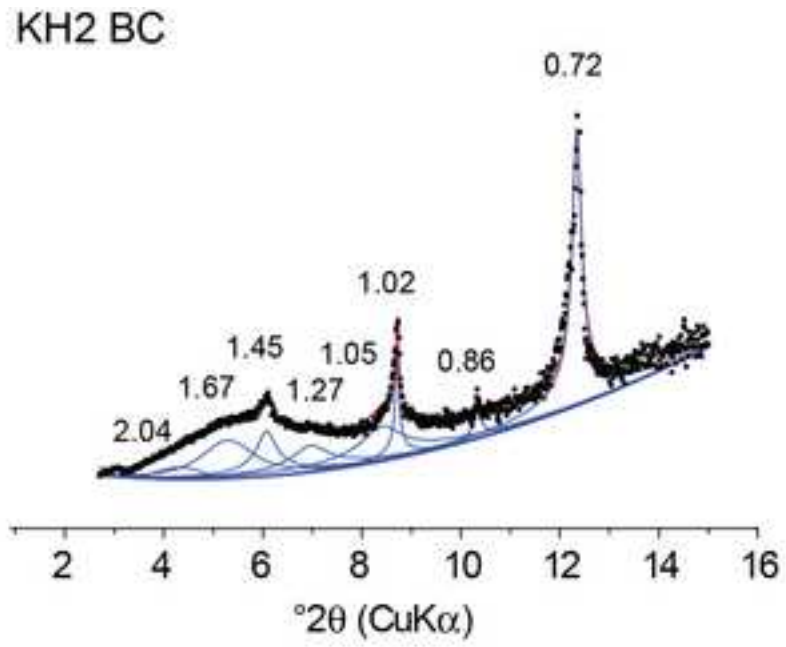

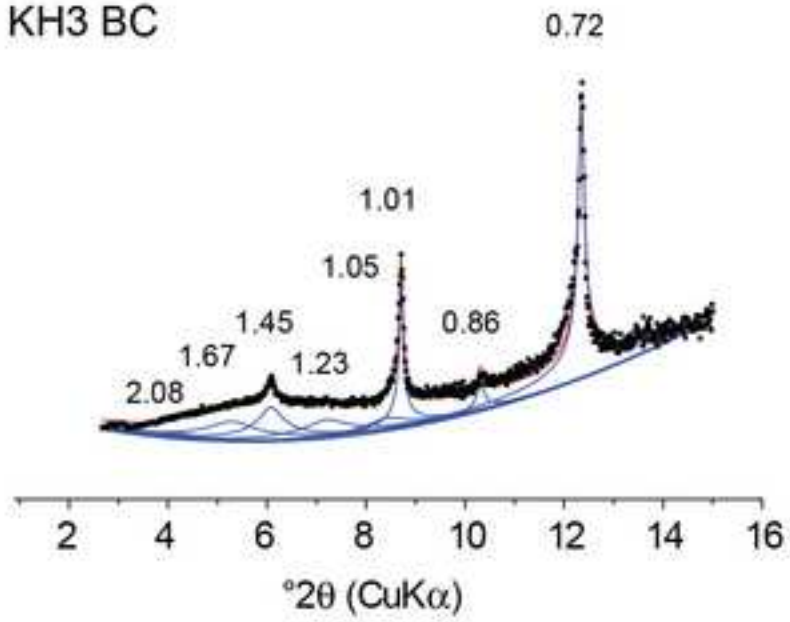

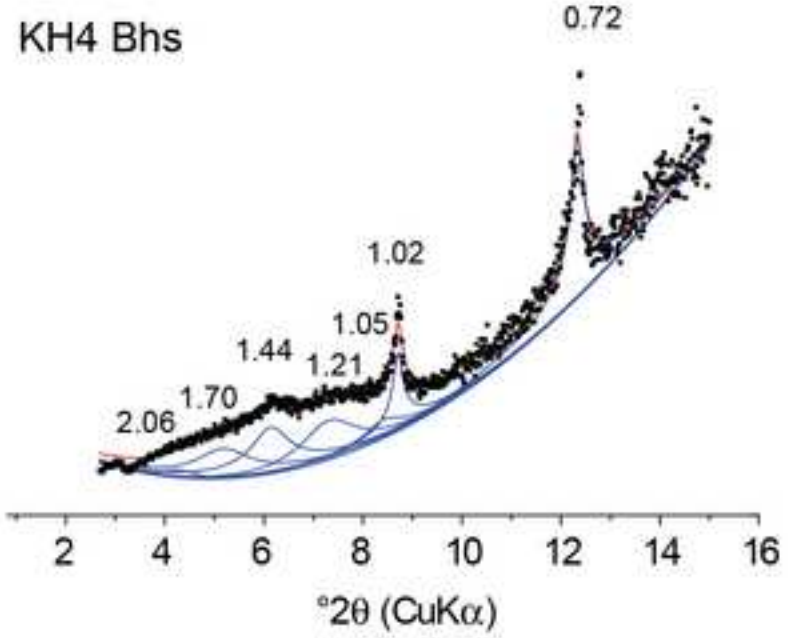

Figure
Click here to download high resolution image

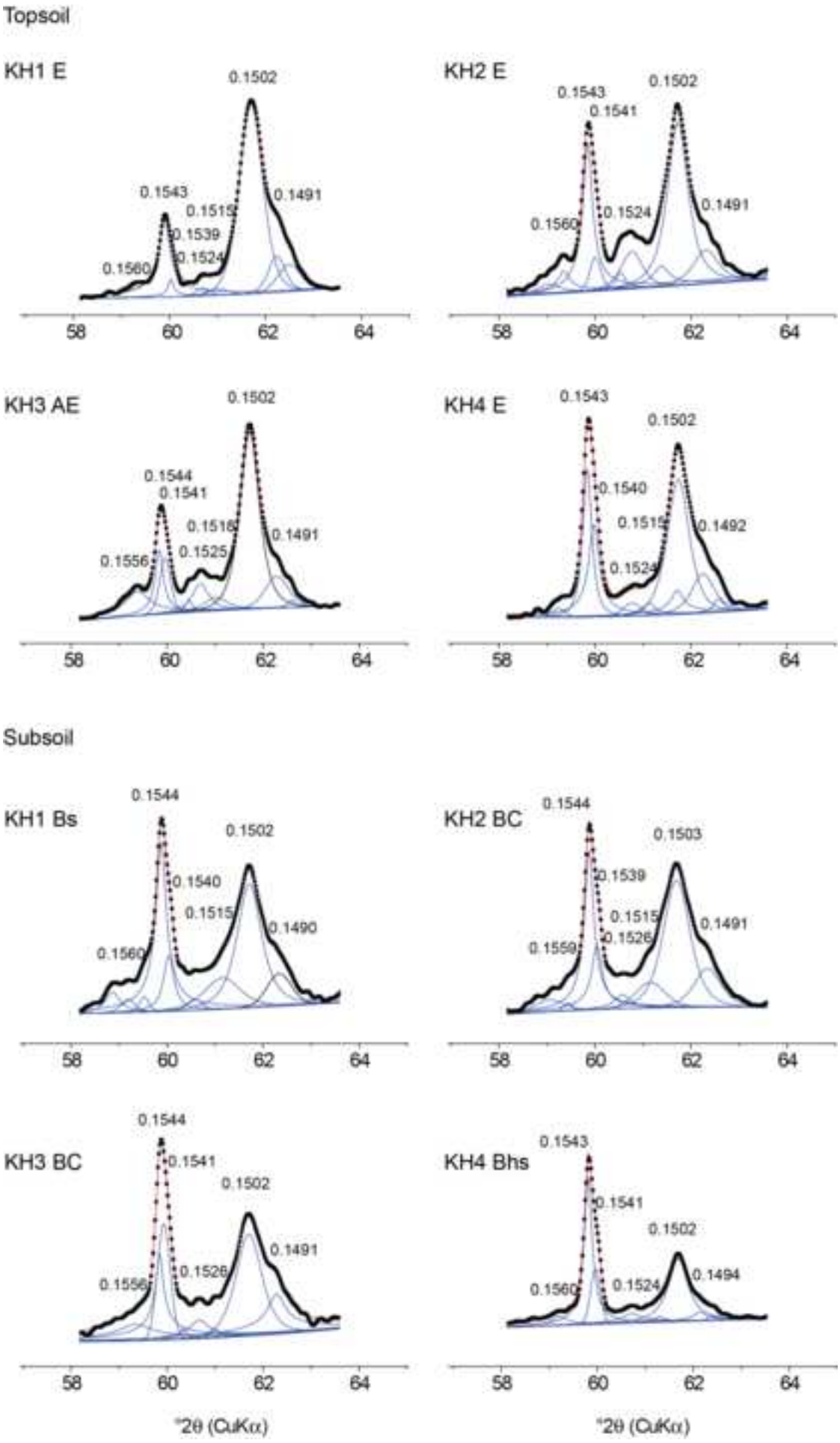

Figure
Click here to download high resolution image

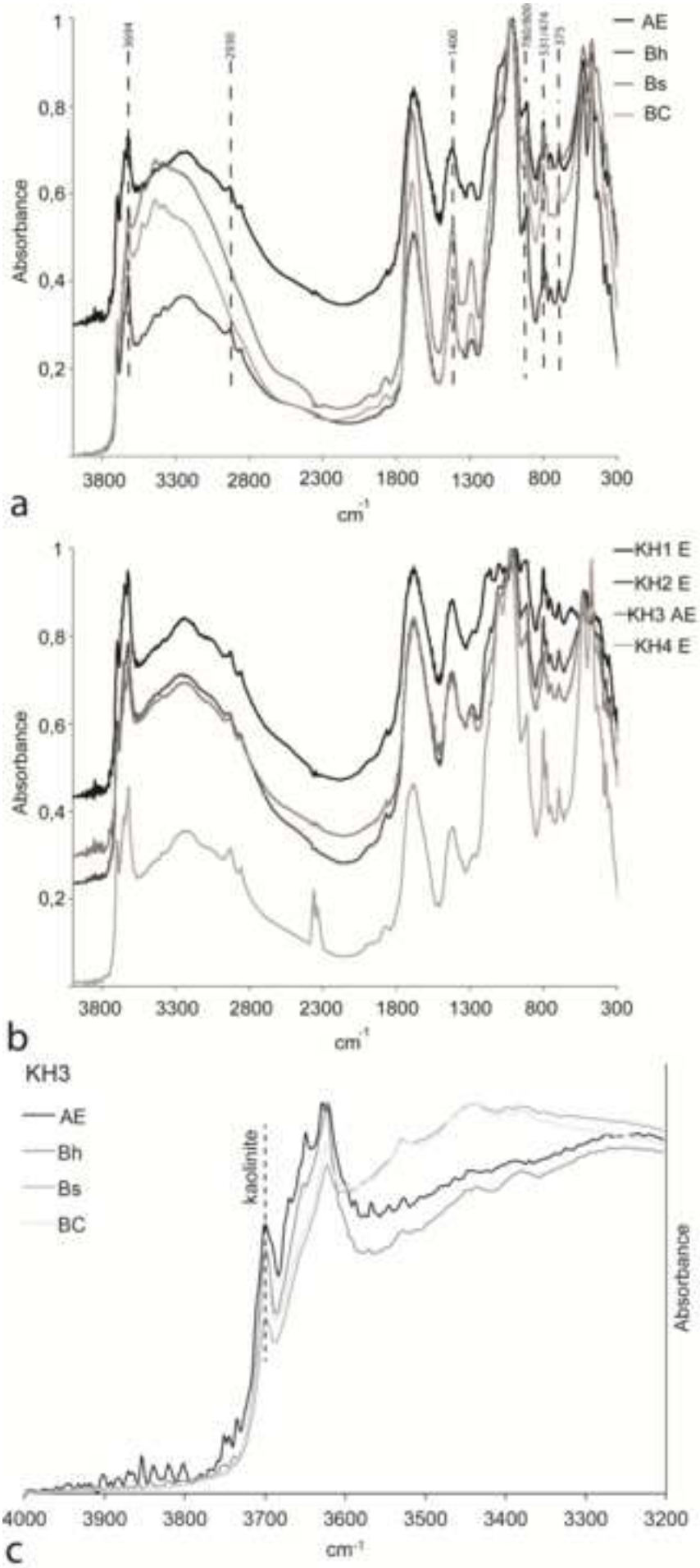

Figure
Click here to download high resolution image